

Testing dark energy models with a new sample of strong-lensing systems

Mario H. Amante^{1*}, Juan Magaña^{2,3,4 †}, V. Motta^{4‡}, Miguel A. García-Aspeitia^{1,5§} and Tomás Verdugo^{6¶}

¹ *Unidad Académica de Física, Universidad Autónoma de Zacatecas,*

Calzada Solidaridad esquina con Paseo a la Bufa S/N C.P. 98060, Zacatecas, México.

² *Instituto de Astrofísica, Pontificia Universidad Católica de Chile, Av. Vicuña Mackenna, 4860, Santiago, Chile.*

³ *Centro de Astro-Ingeniería, Pontificia Universidad Católica de Chile, Av. Vicuña Mackenna, 4860, Santiago, Chile.*

⁴ *Instituto de Física y Astronomía, Facultad de Ciencias,*

Universidad de Valparaíso, Avda. Gran Bretaña 1111, Valparaíso, Chile.

⁵ *Consejo Nacional de Ciencia y Tecnología, Av. Insurgentes Sur 1582.*

Colonia Crédito Constructor, Del. Benito Juárez C.P. 03940, Ciudad de México, México.

⁶ *Instituto de Astronomía, Universidad Nacional Autónoma de México, Apartado postal 106, C.P. 22800, Ensenada, B.C., México*

Accepted YYYYMMDD. Received YYYYMMDD; in original form YYYYMMDD

ABSTRACT

Inspired by a new compilation of strong lensing systems, which consist of 204 points in the redshift range $0.0625 < z_l < 0.958$ for the lens and $0.196 < z_s < 3.595$ for the source, we constrain three models that generate a late cosmic acceleration: the ω -cold dark matter model, the Chevallier-Polarski-Linder and the Jassal-Baglia-Padmanabhan parametrizations. Our compilation contains only those systems with early type galaxies acting as lenses, with spectroscopically measured stellar velocity dispersions, estimated Einstein radius, and both the lens and source redshifts. We assume an axially symmetric mass distribution in the lens equation, using a correction to alleviate differences between the measured velocity dispersion (σ) and the dark matter halo velocity dispersion (σ_{DM}) as well as other systematic errors that may affect the measurements. We have considered different sub-samples to constrain the cosmological parameters of each model. Additionally, we generate a mock data of SLS to assess the impact of the chosen mass profile on the accuracy of Einstein radius estimation. Our results show that cosmological constraints are very sensitive to the selected data: some cases show convergence problems in the estimation of cosmological parameters (e.g. systems with observed distance ratio $D^{obs} < 0.5$), others show high values for the chi-square function (e.g. systems with a lens equation $D^{obs} > 1$ or high velocity dispersion $\sigma > 276$ km s⁻¹). However, we obtained a fiducial sample with 143 systems which improves the constraints on each tested cosmological model.

Key words: gravitational lensing: strong, dark energy, cosmology: observations, cosmology: theory, cosmological parameters.

1 INTRODUCTION

Contrasting cosmological models with modern observations is fundamental to understand the nature of the $\sim 96\%$ of our Universe (Planck Collaboration et al. 2016; Aghanim et al. 2018a) known as the dark sector, which refers to $\sim 26\%$ of the total content in dark matter (DM) the one responsible

for the formation of large-scale structure, and $\sim 69\%$ in dark energy (DE), the possible cause for the current accelerated expansion (Schmidt et al. 1998; Perlmutter et al. 1999; Riess et al. 1998). In the most accepted paradigm, DM is a non-relativistic matter in the decoupling epoch (i.e. cold), and the traditional way to treat the DE nature is through the addition of an effective cosmological constant (CC) in the energy-momentum tensor of the Einstein field equations. The CC origin is related to the quantum vacuum fluctuations, but this hypothesis is plagued by severe pathologies due to its inability to renormalize the energy density of quantum vacuum, obtaining a discrepancy of ~ 120 orders

* E-mail: mario.herrera@fisica.uaz.edu.mx

† E-mail: jmagana@astro.puc.cl

‡ E-mail: veronica.motta@uv.cl

§ E-mail: aspeitia@fisica.uaz.edu.mx

¶ E-mail: tomasv@astro.unam.mx

of magnitude between the theoretical estimations and the cosmological observations (Zeldovich 1968; Weinberg 1989). The CC also has the coincidence problem, i.e. why the Universe transition, from a decelerated to an accelerated phase, is produced at late times.

The CC theoretical problems have led the community to propose a variety of ideas to reproduce the late cosmic acceleration. Some of them postulate the existence of DE, for example, quintessence (Ratra & Peebles 1988; Wetterich 1988), phantom (Chiba et al. 2000; Caldwell 2002) fields, Chaplygin gas (Chaplygin 1904; Kamenshchik et al. 2001; Bilic et al. 2002; Hernandez-Almada et al. 2018), $w(z)$ parameterizations for dynamical DE (Chevallier & Polarski 2001; Linder 2003; Jassal et al. 2005), interacting dark energy (Caldera-Cabral et al. 2009), etc (for a thorough review of all these alternatives see Copeland et al. 2006; Li et al. 2011). Other models modify the Einsteinian gravity to resemble the DE like brane models (García-Aspeitia & Matos 2011; García-Aspeitia et al. 2018a; García-Aspeitia et al. 2018b), $f(R)$ models (Buchdahl 1970; Starobinsky 1980; Sotiriou & Faraoni 2010), scalar-tensor theories (Brans & Dicke 1961; Galiautdinov & Kopeikin 2016; Langlois et al. 2018), Unimodular gravity (Perez & Sudarsky 2017; García-Aspeitia et al. 2019), among others.

On the other hand, observational data are used to test these models. Among the most frequently used are the cosmic microwave background radiation (CMB, Planck Collaboration et al. 2016; Aghanim et al. 2018a), baryonic acoustic oscillations (BAO, Eisenstein et al. 2005; Blake et al. 2012; Alam et al. 2017; Bautista et al. 2017), type Ia Supernovae (SNe Ia, Scolnic et al. 2018) and observational Hubble data (OHD, Jimenez & Loeb 2002; Moresco et al. 2016; Magaña et al. 2018). Consistency in the cosmological parameters among different techniques, rather than more accurate measurements, is desirable to better understand the nature of DE. In the last years, several efforts have been made by the community to include gravitational lens systems in the study of the Universe's evolution. Some of the pioneers are Futamase & Yoshida (2001); Biesiada (2006), who used only one strong-lens system to study some of the most popular cosmological models. Grillo et al. (2008) introduced a methodology to estimate cosmological parameters using Strong Lensing Systems (SLS) (see also Jullo et al. 2010; Magaña et al. 2015, 2018). They apply the relation between the Einstein radius and the central stellar velocity dispersion assuming an isothermal profile for the total density distribution of the lens (elliptical) galaxy. Their simulations found that the method is accurate enough to obtain information about the underlying cosmology. They concluded that the stellar velocity dispersion and velocity dispersion of the isothermal lens model are very similar in the w cold dark matter (w CDM) model. Biesiada et al. (2010) used the same procedure comparing a distance ratio, D^{obs} , constructed from SLS observations such as the Einstein radius and spectroscopic velocity dispersion of the lens galaxy, with a theoretical counterpart, D^{th} . By using a sample containing 20 SLS, they demonstrated that this technique is useful to provide insights into DE. Cao et al. (2012) updated the sample to 80 systems and proposed a modification that takes into account deviations from sphericity, i.e. from the singular isothermal sphere (SIS). Later on, Cao et al. (2015) considered lens profile deviations due to the redshift evolution

of elliptical galaxies by using spherically symmetric power-law mass distributions for the lenses and also increased the compilation up to 118 points. They also explore the consequences of using aperture-corrected velocity dispersions on the parameter estimations. Some authors have pointed out the need for a sufficiently large sample to test DE models with higher precision (Yennapureddy & Melia 2018). For instance, Melia et al. (2015) have emphasized that a sample of ~ 200 SLS can discern the $R_h = ct$ model from the standard one. Qi et al. (2018) simulated strong lensing data to constrain the curvature of the Universe and found that, by increasing the sample (16000 lenses) and combining with compact radio quasars, it could be constrained with an accuracy of $\sim 10^{-3}$. Recently, Leaf & Melia (2018) have revisited this cosmological tool with the largest sample of SLS (158) until now, including 40 new systems presented by Shu et al. (2017). The authors proposed a new approach to improve this technique by introducing in the observational distance ratio error (δD^{obs}), a parameter σ_x to take into account the SIE scatter and any other source of errors in the measurements. In their analysis, they excluded 29 SLS that are outside the region $0 < D_{obs} < 1$, and the system SL2SJ085019-034710 (Sonnenfeld et al. 2013b) which seems to be an extreme outlier for their models. Their results show that a $\sigma_x = 12.2\%$ provides more statistically significant cosmological constraints. Finally, Chen et al. (2018) used 157 SLS to analyze the Λ CDM model. They considered a lens mass distribution $\rho(r) = \rho_0 r^{-\gamma}$ and three possibilities for the γ parameter: a constant value, a dependence with the lens redshift (z_l), and a dependence with both the surface mass density and the lens redshift. They concluded that although Ω_{om} , used as the only free parameter in Λ CDM scenario, is very sensitive to the lens mass model, it provides weak constraints which are also in tension with Planck measurements.

In this work we compile a new sample of 204 strong gravitational lens systems, which have been measured by different surveys: Sloan Lens ACS survey (SLACS Bolton et al. 2006); BOSS Emission-Line Lens Survey (BELLS Brownstein et al. 2012a); CfA-Arizona Space Telescope LENS Survey (CASTLES Muñoz et al. 1998); Lenses Structure and Dynamics survey (LSD Treu & Koopmans 2004); CFHT Strong Lensing Legacy Survey (SL2S Cabanac et al. 2007); Strong-lensing Insights into Dark Energy Survey (STRIDES Treu et al. 2018). We have added 47 systems to the last compilation Chen et al. (2018) with the aim to constrain the parameters for the w cold dark matter (w CDM) model, the Chevallier-Polarski-Linder (CPL) and Jassal-Baglia-Padmanabhan (JBP) parameterizations of the DE equation of state.

The paper is organized as follows. In Sec. 2 we show the data for the strong lensing cosmological observations. In Sec. 3 we present the Friedmann equations for the models and parametrizations mentioned previously. In section 4 we introduce the criteria to assess the goodness-of-fit for each case. In section 5 our results are shown and finally in section 6 we present the conclusions and perspectives.

2 STRONG LENSING AS A COSMOLOGICAL TEST

2.1 Methodology

Strong lensing systems have been used over the years to constrain cosmological parameters and supply an alternative way to understand the nature of dark energy (Biesiada 2006; Biesiada et al. 2010; Cao et al. 2012; Cao et al. 2015; Jullo et al. 2010; Magaña et al. 2015, 2018). In this paper we gather new data from SLS, making a catalog with 204 systems. This compilation allow us to analyze cosmological models with more precision and compare with other astrophysical tools as standard candles or standard rulers (Scolnic et al. 2018; Blake et al. 2012; Alam et al. 2017; Bautista et al. 2017). When a galaxy acts as a lens, the separation among the multiple-images depends on the deflector mass and the angular diameter distances to the lens and to the source. When a lens is described by a Singular Isothermal Sphere (SIS), the Einstein radius is defined as (Schneider et al. 1992)

$$\theta_E = 4\pi \frac{\sigma_{SIS}^2 D_{ls}}{c^2 D_s}, \quad (1)$$

where σ_{SIS} is the velocity dispersion of the lensing galaxy, c is the speed of light, D_s is the angular diameter distance to the source, and D_{ls} the angular diameter distance between the lens and the source. The enclosed projected mass inside the Einstein radius (θ_E) is independent of the mass profile (Schneider et al. 1992), generally estimated using an isothermal-ellipsoid mass distribution (SIE). Furthermore, it has been demonstrated that the lensing mass distribution of early-type galaxies is very close to isothermal (Kochanek 1995; Muñoz et al. 2001; Rusin et al. 2002; Treu & Koopmans 2002; Koopmans & Treu 2003a; Rusin et al. 2003b; Grillo et al. 2008).

Since the angular diameter distance D , in terms of redshift z is defined as

$$D(z) = \frac{c}{H_0(1+z)} \int_0^z \frac{dz'}{E(z')}, \quad (2)$$

being H_0 the Hubble constant, then the Einstein radius depends on the cosmological model through the dimensionless Friedmann equation $E(z)$. By defining a theoretical distance ratio $D^{th} \equiv D_{ls}/D_s$, we obtain

$$D^{th}(z_l, z_s; \Theta) = \frac{\int_{z_l}^{z_s} \frac{dz'}{E(z', \Theta)}}{\int_0^{z_s} \frac{dz'}{E(z', \Theta)}}, \quad (3)$$

where Θ is the free parameter vector for any underlying cosmology, z_l and z_s are the redshifts to the lens and source respectively. On the other hand, its observable counterpart can be computed as

$$D^{obs} = \frac{c^2 \theta_E}{4\pi \sigma^2}, \quad (4)$$

where σ is the measured velocity dispersion of the lens dark matter halo. Therefore, the compilation of SLS with their measurements for σ and θ_E can be used to estimate cosmological parameters (Grillo et al. 2008) by minimizing the following chi-square function,

$$\chi_{SL}^2(\Theta) = \sum_{i=1}^{N_{SL}} \frac{[D^{th}(z_l, z_s; \Theta) - D^{obs}(\theta_E, \sigma^2)]^2}{(\delta D^{obs})^2}, \quad (5)$$

where the sum is over all the (N_{SL}) lens systems and δD^{obs} is the uncertainty of each D^{obs} measurement which can be computed employing the standard way of error propagation as

$$\delta D^{obs} = D^{obs} \sqrt{\left(\frac{\delta \theta_E}{\theta_E}\right)^2 + 4 \left(\frac{\delta \sigma}{\sigma}\right)^2}, \quad (6)$$

being $\delta \theta_E$ and $\delta \sigma$ the error reported for the Einstein radius and velocity dispersion respectively.

One of the advantages of this method is its independence of the Hubble constant H_0 , as it is eliminated in the ratio of two angular diameter distances (see Eq. 1). Hence, the tension of H_0 between some of the most reliable measurements (Riess et al. 2016; Aghanim et al. 2018b; Riess et al. 2019) is not a problem for this method since it is not necessary to assume any H_0 initial value. Some disadvantages are: its dependency on the lens model fitted to the data to obtain the Einstein radius (e.g. Cao et al. 2015), the spectroscopically measured stellar velocity dispersion (σ) that might not be the same as the dark matter halo velocity dispersion σ_{DM} , and any other systematic error that could change the separation between images or the observed σ . Consequently, we take into account these uncertainties by introducing the parameter f into the relation $\sigma_{DM} = f\sigma$, thus Eq. (1) is

$$D^{obs} = \frac{c^2 \theta_E}{4\pi \sigma^2 f^2}. \quad (7)$$

Ofek et al. (2003) estimate that those systematics might affect the image separation $\Delta\theta$ up to $\sim 20\%$ (since $\Delta\theta \propto \sigma^2$), and thus assume the constraints $(0.8)^{1/2} < f < (1.2)^{1/2}$. Moreover, Treu et al. (2006) claim that, for systems with velocity dispersion between $200 - 300 \text{ km s}^{-1}$, there is a relation between the measurement of σ_{spec} from spectroscopy and those estimated from the lens model

$$\langle f_{SIE} \rangle = \frac{\sigma_{spec}}{\sigma_{SIE}} \approx 1.010 \pm 0.017, \quad (8)$$

where σ_{SIE} is the velocity dispersion obtained from a singular isothermal ellipsoid, and it is also consistent with Ofek et al. (2003) results. Notice that Treu et al. (2006) relation cannot be used in our case because: a) σ for several objects fall outside the interval of validity, and b) it was obtained assuming a Λ CDM model, and thus it could introduce another source of bias in our estimations. Therefore, hereafter we use Ofek et al. (2003) estimation for f . We also investigate the repercussions of assuming f as an independent parameter for each SLS to estimate cosmological parameters (see Appendix B). In addition, we analyze a mock catalog of 788 SLS to assess the impact on the Einstein radius estimation when using an isothermal profile instead of a more complex model (7) (see Appendix C).

On the other hand, for some SLS we obtain incorrect $D_{obs} > 1$ values (i.e. $D_{ls} > D_s$, see Table A2). Leaf & Melia (2018) point out that these values are theoretically unphysical, thus they should be either disregarded or corrected by introducing an extra source of error (e.g. δD^{obs}). However, as the source of such behavior is unknown, we choose to keep these observed systems throughout our analysis (without introducing the suggested δD^{obs} error) and, instead, offer the parameter estimations with and without those systems for comparison. In the following section we

present the data that will be used in the chi-square function (Eq. 5) to test DE models.

2.2 Data

In this section we describe our new compilation of SLS. To construct D^{obs} we have chosen only systems with spectroscopically data well measured from different surveys. We have considered 19 SLS from the CASTLES, 107 from SLACS, 38 from BELLS, 4 from LSD, 35 from SL2S and one system from the DES survey. The final list has a total of 204 systems, being the largest sample of SLS to date. We use spectroscopy to select those lenses with lenticular (S0) or elliptical (E) morphologies which have been modeled assuming a SIS ($\sim 3\%$) or SIE ($\sim 97\%$) lens model. Many systems have not been taken into account due to several issues. For instance, the system PG1115+080 (Tonry 1998) from the CASTLES survey has been discarded because the lens mass model is steeper than isothermal. In addition, the system MGJ0751+2716 (Spingola et al. 2018) was also discarded because the main lens belongs to a group of galaxies. From the SLACS survey (Bolton et al. 2008; Auger et al. 2009), we remove the systems SDSSJ1251-0208, SDSSJ1432+6317, SDSSJ1032+5322 and SDSSJ0955+0101 since the lens galaxies are late-type. The same reason is applied to the systems SDSSJ1611+1705 and SDSSJ1637+1439 from the BELLS survey (Shu et al. 2016). We have also discarded the systems SDSSJ2347-0005 and SDSSJ0935-0003 from the SLACS survey and the system SDSSJ11040.42+364924.4 from the BELLS survey because they have large measured velocity dispersions ($\sim 400\text{km s}^{-1}$ or bigger values), suggesting the lens might be part of a group of galaxies or that there is substructure in the line-of-sight. For those systems without reported velocity dispersion error, we assumed the average error of the measurements in the survey subsample as follows. For the 9 systems from CASTLES we consider the average error on σ for this survey, i.e. a 14 %. In the case of the system DES J2146-0047 (Agnello et al. 2015), we have assumed a 10% error on σ , which is the average error of the entire sample. The LSD survey (Koopmans & Treu 2003b; Treu & Koopmans 2004) reports σ corrected by circular aperture using the expression obtained by Jorgensen et al. (1995a,b). A close inspection of the σ_{spec} values, with and without aperture correction, presented by Cao et al. (2015) show the difference is smaller than reported error. Thus, we decided to use the observed values (σ) and the reported error for the sample without the aperture correction. On the other hand, in those systems in which the Einstein radius error was not reported, we followed Cao et al. (2015) and assumed an error of $\delta\theta_E = 0.05$, which is the average value of the systems with reported errors in this sample.

Our final sample (FS) is presented in Table A1, having a total of 204 data points whose lens and source redshifts are in the ranges $0.0625 < z_l < 0.958$ and $0.196 < z_s < 3.595$, respectively. All the systems for which we assumed a velocity dispersion error are marked in the sample.

In addition, we have constructed the following subsamples to test the impact on the parameter estimation for the different DE models. We divide the sample into different regions according to the observed value for the distance ratio

D^{obs} , because there are systems that do not fall in a physical region. We also split the sample into different regions according to the redshift of the lens galaxy to check for any significant changes in the estimation of cosmological parameters associated to the deflector position. Finally, following Chen et al. (2018), we also separate the systems in distinct sub-samples according to the measured velocity dispersion. We name the sub-samples as follows:

- SS1: 172 data points with $D^{obs} \leq 1$
- SS2: 29 data points with $D^{obs} < 0.5$
- SS3: 143 data points in $0.5 \leq D^{obs} \leq 1$
- SS4: 32 data points with $D^{obs} > 1$
- SS5: 64 data points with $\sigma < 210 \text{ km s}^{-1}$
- SS6: 53 data points in $210 \text{ km s}^{-1} \leq \sigma < 243 \text{ km s}^{-1}$
- SS7: 49 data points in $243 \text{ km s}^{-1} \leq \sigma \leq 276 \text{ km s}^{-1}$
- SS8: 38 data points with $\sigma > 276 \text{ km s}^{-1}$
- SS9: 52 data points with $D^{obs} \leq 1$ and $z_l < 0.2$
- SS10: 48 data points with $D^{obs} \leq 1$ and $0.2 \leq z_l \leq 0.4$
- SS11: 72 data points with $D^{obs} \leq 1$ and $z_l > 0.4$

3 COSMOLOGICAL MODELS

Hereafter we consider the following models with flat geometry that contain dark and baryonic matter and dark energy, neglecting the density parameter of radiation because its contribution at low redshifts is of the order of $\sim 10^{-5}$.

• The ω CDM cosmology.- This model is the simplest extension to the CC. The dark energy has a constant EoS but it deviates from $w_0 = -1$, and should satisfy $\omega_0 < -1/3$ to obtain an accelerated Universe. The equation $E(z)$ can be written as:

$$E(z)_\omega^2 = \Omega_{m0}(1+z)^3 + (1 - \Omega_{m0})(1+z)^{3(1+\omega_0)}, \quad (9)$$

where Ω_{m0} is the matter density parameter at $z = 0$ and the deceleration parameter reads

$$q(z)_\omega = \frac{1}{2E(z)_\omega^2} \left[3\Omega_{m0}(1+z)^3 + 3(1+\omega_0)(1 - \Omega_{m0})(1+z)^{3(1+\omega_0)} \right] - 1. \quad (10)$$

• The CPL parametrization.- An approach to study dynamical DE models is through a parametrization of its equation of state. One of the most popular is proposed by Chevallier & Polarski (2001); Linder (2003), and reads as

$$\omega(z) = \omega_0 + \omega_1 \frac{z}{(1+z)}, \quad (11)$$

where ω_0 is the EoS at redshift $z = 0$ and $\omega_1 = dw/dz|_{z=0}$. The dimensionless $E(z)$ for the CPL parametrization is

$$E(z)_{CPL}^2 = \Omega_{m0}(1+z)^3 + (1 - \Omega_{m0})(1+z)^{3(1+\omega_0+\omega_1)} \exp\left(\frac{-3\omega_1 z}{1+z}\right), \quad (12)$$

the $q(z)$ is written in the form

$$q(z)_{CPL} = \frac{1}{2E(z)_{CPL}^2} \left[3\Omega_{m0}(1+z)^3 + 3(1 - \Omega_{m0})(1 + w_0 + w_1)(1+z)^{3(1+\omega_0+\omega_1)} \times \exp\left(\frac{-3\omega_1 z}{1+z}\right) - 3w_1(1 - \Omega_{m0})(1+z)^{3(1+\omega_0+\omega_1)-1} \times \exp\left(\frac{-3\omega_1 z}{1+z}\right) \right] - 1. \quad (13)$$

Table 1. ΔAIC and ΔBIC criteria.

ΔAIC	Empirical support for model i
0 - 2	Substantial
4 - 7	Considerably less
> 10	Essentially none
ΔBIC	Evidence against model i
0 - 2	Not worth more than a bare mention
2 - 6	Positive
6 - 10	Strong
> 10	Very strong

• The JBP parametrization.- Jassal et al. (2005) proposed the following *ansatz* to parametrize the dark energy EoS

$$\omega(z) = \omega_0 + \omega_1 \frac{z}{(1+z)^2}, \quad (14)$$

where ω_0 is the EoS at redshift $z = 0$ and $\omega_1 = dw/dz|_{z=0}$. The dimensionless $E(z)$ for the JBP parametrization is

$$E(z)_{JBP}^2 = \Omega_{m0}(1+z)^3 + (1 - \Omega_{m0})(1+z)^{3(1+\omega_0)} \exp\left(\frac{3\omega_1 z^2}{2(1+z)^2}\right), \quad (15)$$

the deceleration parameter reads

$$q(z)_{JBP} = \frac{1}{2E(z)_{JBP}^2} \left[3\Omega_{m0}(1+z)^3 + 3(1 - \Omega_{m0})(1 + \omega_1)(1+z)^{3(1+\omega_1)} \times \exp\left(\frac{3\omega_1 z^2}{2(1+z)^2}\right) + 3\omega_1(1 - \Omega_{m0})z(1+z)^{3(1+\omega_1)-2} \times \exp\left(\frac{3\omega_1 z^2}{2(1+z)^2}\right) \right] - 1. \quad (16)$$

Therefore, it may be possible to reconstruct the $q(z)$ by constraining the parameters for each model and determine whether the Universe experiments an accelerated phase at late times.

4 MODEL SELECTION

To compare among the different DE models, we use the Akaike information criterion (AIC, Akaike 1974) and Bayesian information criterion (BIC, Schwarz 1978) defined as:

$$\text{AIC} = \chi_{min}^2 + 2k, \quad (17)$$

$$\text{BIC} = \chi_{min}^2 + k \ln N, \quad (18)$$

where χ_{min}^2 is the chi-square obtained from the best fit of the parameters, k is the number of parameters and N the number of data points used in the fit. A model with smaller AIC and BIC is more favored. Notice that the AIC (BIC) absolute value is irrelevant, the important quantity is the relative value of AIC (BIC) for the model i with respect to the minimum AIC_{min} (BIC_{min}) among all the models. Table 1 shows the $\Delta\text{AIC} = \text{AIC}_i - \text{AIC}_{min}$ and $\Delta\text{BIC} = \text{BIC}_i - \text{BIC}_{min}$ criteria. (see Shi et al. 2012, and references therein for further details).

In addition, to measure the quality of our cosmological constraints we use the FOM estimator

$$\text{FoM} = \frac{1}{\sqrt{\det \text{Cov}(f1, f2, f3, \dots)}}, \quad (19)$$

where $\text{Cov}(f1, f2, f3, \dots)$ is the covariance matrix of the cosmological parameters f_i (Wang 2008). This indicator is a generalization of those proposed by Albrecht et al. (2006), and larger values imply stronger constraints on the cosmological parameters since they correspond to a smaller error ellipse.

5 RESULTS

In the parameter estimation we have considered the Gaussian likelihood $\mathcal{L}(\Theta) \propto e^{-\chi_{\text{SL}}^2(\Theta)}/2$, where the $\chi_{\text{SL}}^2(\Theta)$ is given by Eq. (5). The free parameters Θ for each model were estimated through a MCMC Bayesian statistical analysis. We used the Affine Invariant Markov chain Monte Carlo (MCMC) Ensemble sampler from the `emcee` (Foreman-Mackey et al. 2013) Python module. We considered 1000 (burn-in-phase) steps to approach the region of the mean value, 5000 MCMC steps and 1000 walkers initialized close to the region of maximum probability according to other astrophysical observations. We check the convergence of the chains using the Gelman-Rubin test proposed by Gelman & Rubin (1992), stopping the burn-in-phase if all the parameters are less than 1.07.

In each model, we have considered thirteen tests in the Bayesian analysis. The first test was performed employing the FS using the SIS approach given by Eq. 4; the second test was done using the SS1 sample; and the third test was carried out on the FS sample adding a new parameter (f) that takes into account unknown systematics as was previously mentioned in equation (7). We also performed tests with the SLS data binned in D^{obs} : the samples SS2, SS3 and SS4. In addition, we estimated the model parameters with the SLS data binned in σ using: the SS5 sample; the SS6 sample; the SS7 sample; and the SS8 sample. Finally, we constrained the model parameters with the SLS data binned in the lens redshift (z_l) for: the SS9 sample, the SS10 sample, and the SS11 sample. These tests were carried out assuming a gaussian prior for $\Omega_{0m} = 0.3111 \pm 0.0056$, according to the most recent observations from Planck 2018 (Aghanim et al. 2018a). We also assume the following priors: $-4 < \omega_0 < 1$, $-5 < \omega_1 < 5$ and $(0.8)^2 < f < (1.2)^2$. Table 2 provides the mean values for the free parameters of each model using the different cases mentioned above. The error propagation was performed through a Monte Carlo approach at 1σ confidence level. We also present the values for χ_{min}^2 and $\chi_{red}^2 = \chi_{min}^2/(N - k)$, where N and k are the number of data points and parameters used in each scenario (see section 4). Table 3 gives the AIC, BIC, and FOM values for each cosmological model using the results of the FS, FS+f, SS3 analysis.

5.1 The ωCDM constraints

For the ωCDM model, we considered two free parameters Ω_{0m} and ω_0 , additionally we consider an extra parameter f only in one case (FS). As we mentioned earlier, a Gaussian prior on Ω_{0m} is assumed, hence our attention is focused on the ω_0 parameter. We found consistency for the constraints obtained in the first three tests (see figure 1, upper-left and lower panels), i.e. the ω_0 value is not affected whether a

new extra parameter f is considered or the systems with $D^{obs} > 1$ are excluded. However, the χ_{min}^2 and χ_{red}^2 values reflect the goodness of the constraints: improvement when we exclude the systems in the region of $D^{obs} > 1$, and without significant change when we consider the corrective parameter f , in agreement with previous studies ($f \sim 1$; $f = 1.010 \pm 0.017$ for Cao et al. 2012; Treu et al. 2006, respectively). However, when different sub-samples are considered (see figure 1, upper-right and middle panels) ω_0 seems to have different values, the majority pointing to an Universe with a phantom DE, and two cases (SS2 and SS8) where ω_0 is positive, which does not satisfies the accelerated condition $\omega_0 < -1/3$, yielding an unphysical $q(z)$ (see Figure 2, upper panel). In the following, we discuss in further detail some key results obtained from the sub-samples.

The SS2 was done using systems in the region of $D^{obs} < 0.5$, this sub-sample consist of 29 points, eight of them have the peculiarity that their theoretical lens equation Eq. (3) provides $D^{th} < 0.5$ only when ω_0 becomes positive. However, three of these systems (MG0751+2716, SL2SJ085019–034710, and SL2SJ02325–040823) never enter the aforementioned region. These are consequences of the functional form for D^{th} , which gives the same result for different values of ω_0 . As a repercussion, cosmological parameters show convergence problems with the MCMC, e.g. notice that the $\Omega_{m0}-\omega_0$ posterior distribution presents double contours (see figure 1, upper-right panel).

The SS8 considers systems with velocity dispersions for the lens galaxies in the region of $\sigma > 276 \text{ km s}^{-1}$. This case gives larger χ_{red}^2 values than previous tests, indicating an Universe without an acceleration stage within 3σ error. The $D^{obs} > 1$ (SS4) region presents the highest χ_{red}^2 value for the ω CDM model. These issues indicate that some systems within this regions could have some uncertainties affecting the measured quantities θ_E and σ . Appendix A2 shows different kinds of systematics affecting the measurements for the $D^{obs} > 1$ region.

Finally, we examined three different regions according to the lens galaxy redshift, excluding those systems with $D^{obs} > 1$. We found that: $0.2 \leq z_l \leq 0.4$ presents the worst constraints, although with similar values to those obtained using the complete sample; $z_l < 0.2$ and $z_l > 0.4$ show the second and third best constraints (see χ_{red}^2 values in table 2). In general, we obtain a good fit to the data and the worst results (higher χ_{red}^2) are those corresponding to the sub-samples: $D^{obs} > 1$ (SS4), $\sigma < 210 \text{ km s}^{-1}$ (SS5) and $\sigma > 276 \text{ km s}^{-1}$ (SS8). The best χ_{red}^2 value is obtained using SS3, i.e when $0.5 < D^{obs} < 1$.

For most of the tests, the estimated values for the ω_0 constraints deviate from the concordance Λ CDM model ($\omega_0 = 1$) towards the phantom region. When the complete sample is used, our ω_0 bounds (~ -2.5) are inconsistent with $\omega_0 = -0.978 \pm 0.059$, $\omega_0 = -1.56 \pm 0.54$ and $\omega_0 = -1.026 \pm 0.041$, obtained by Abbott et al. (2019); Aghanim et al. (2018b); Scolnic et al. (2018) respectively. However, our best $\omega_0 = -1.653_{-0.322}^{+0.264}$ constraint obtained for $0.5 \leq D^{obs} < 1$ (SS3) is consistent with the aforementioned values and those obtained by Cao et al. (2012) ($\omega_0 = -1.15_{-0.35}^{+0.34}$) using the same method (46 SLS) with a corrective parameter f , and Cao et al. (2015) ($\omega_0 = -1.48_{-0.94}^{+0.54}$) assuming a generalization of the mass distribution (118 SLS). To judge the quality of our constraints we also cal-

culate the FOM (Eq. 19) for each test. The strongest constraints (i.e highest FOM) are obtained when $0.5 \leq D^{obs} < 1$ (see table 3). On the other hand, the $D^{obs} < 0.5$ region provides the least reliable constraints, as expected from the convergence problems and the double confidence contours (see Figure 1 for details).

We present the reconstruction of the ω CDM deceleration parameter in figure 2 (upper panel) using the constraints obtained in each test. Notice that both SS2 and SS8 constraints exhibit unphysical values, i.e. they do not provide an acceleration stage and their $q(z)$ are in disagreement with the standard theoretical prediction at high redshifts ($q(z) \rightarrow 0.5$). The constraints obtained from other samples provide an accelerated phase at late times. However, only SS11 yields a $q_0 = q(z=0)$ value in agreement with the standard model ($q_{0\Lambda\text{CDM}} \sim -0.5$), while the remaining sample values are in tension with the standard one.

5.2 The CPL constraints

Notice that despite the CPL parametrization for the DE EoS (Eq. 11) adds an extra free parameter compared to the ω CDM one, the range of values for χ_{min}^2 and χ_{red}^2 are roughly similar. The ω_0 constraints estimated with the FS (with and without f) and the SS1 are very similar ($\sim -2.3, -2.7$), a straightforward comparison among ω_1 values is not possible because the bounds are different for each scenario (see figure 3, upper-left and lower panels), but showing consistency at 1σ of confidence level. When sub-samples are considered (SS2 to SS11, figure 3, upper-right and middle panels), ω_0 is positive only for the region $z_l > 0.4$ (see middle-right panel), and adopts negative values for the other sub-samples. The ω_1 parameter is very sensitive to all cases having different mean values in each test, however most being consistent at 1σ of confidence level.

When a new parameter f , (FS) is added, no substantial improvements on χ_{red}^2 value is shown. The result for the corrective parameter f is consistent with the ones obtained by Cao et al. (2012); Treu et al. (2006). Once again, the ω_0 and ω_1 constraints seem to get worse in the region $D^{obs} < 0.5$ (SS2), showing convergence problems reflected in double contours in the correlation of the cosmological parameters (see figure 3, upper-right panel). Notice that χ_{red}^2 values higher than the one obtained for the entire sample (table 2) are achieved only in the regions: $D^{obs} > 1$ (SS4), $\sigma < 210 \text{ km s}^{-1}$ (SS5) and $\sigma > 276 \text{ km s}^{-1}$ (SS8). On the other hand, the smallest χ_{red}^2 value is reached in the region of $0.5 < D^{obs} < 1$ (SS3), suggesting a better model fitting.

When the complete sample is used, the ω_0 and ω_1 constraints are not consistent with the observations of Scolnic et al. (2018); Aghanim et al. (2018b) ($\omega_0 = -1.009 \pm 0.159$, $\omega_1 = -0.129 \pm 0.755$ and $\omega_0 = -0.961 \pm 0.077$, $\omega_1 = -0.28 \pm 0.29$, respectively) but show consistency at 1σ with those obtained by Cao et al. (2012) ($\omega_0 = -0.024 \pm 2.42$, $\omega_1 = -6.35 \pm 9.75$) using 46 SLS. In spite of this, some sub-samples are consistent with the works of Scolnic et al. (2018); Aghanim et al. (2018b), showing different behaviors for the DE (phantom and quintessence regime). The ω_0 parameter adopt a positive value in the region $z_l > 0.4$, a similar value is reported in the work of Cao et al. (2012) using a sample with 80 SLS. For all the tests, the FOM estimator gives tight constraints in the $0.2 \leq z_l \leq 0.4$ region (SS10), and

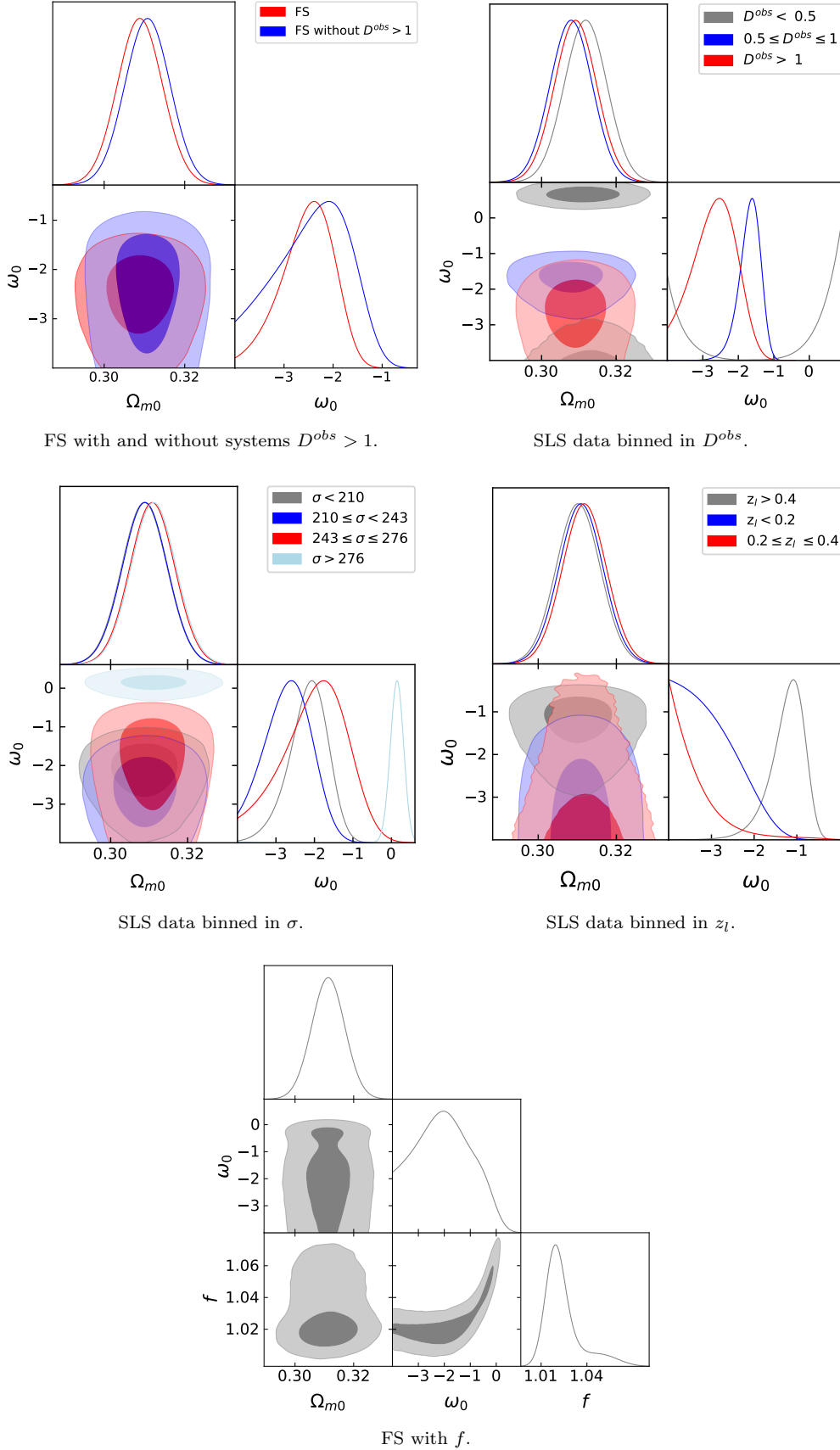


Figure 1. 1D marginalized posterior distributions and the 2D 68%, 99.7% confidence levels for the Ω_{m0} and ω_0 parameters of the ω CDM model and f parameter (lower panel) for the different samples presented in Table 2.

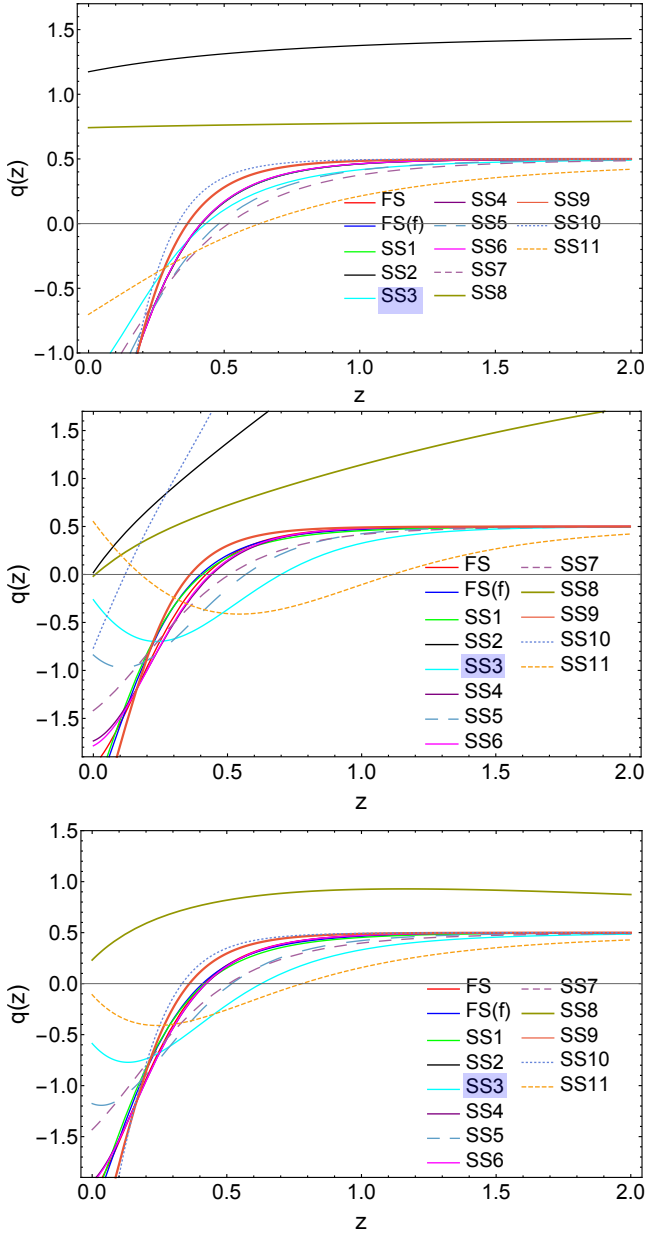


Figure 2. Reconstruction of the $q(z)$ parameter, using data constraints for ω CDM (upper panel), CPL (middle panel) and JBP (lower panel) models. In the JBP case (lower panel), notice that SS2 it is outside the range shown in the figure, in this case SS2 does not predicts an accelerated universe and therefore it is not inside of the labels. Remarking SS3 as the best sample for our analysis.

poor constraints in the region $243\text{km s}^{-1} < \sigma \leq 276\text{km s}^{-1}$ (SS7).

We reconstruct the $q(z)$ function for CPL model using the constraints obtained for each test (see figure 2, middle panel). Notice that SS2, SS8 and SS10 yield constraints that result in unphysical behaviours for $q(z)$. On the contrary, those provided by SS3, SS5 and SS11 source an acceleration-deceleration stage which is characteristic of models where the DE EoS is parametrized, i.e. a slowing down of cosmic acceleration (Cárdenas & Rivera 2012; Cárdenas et al. 2013; Magaña et al. 2014; Wang et al. 2016; Zhang & Xia 2018).

Although SS11 constraints produce an acceleration phase in the Universe, it does not occurs at $z = 0$.

5.3 The JBP constraints

The free parameters of the JBP parametrization are Ω_{0m} , ω_0 and ω_1 . It is worth to notice that the range of values for χ_{min}^2 and χ_{red}^2 are similar to those obtained for the ω CDM and CPL models. For the FS (with and without f) and SS1, although the ω_0 constraints differ slightly, they locate on the phantom regime (see Table 2, figure 4 upper-left and lower panels). The ω_1 parameter has remarkable changes in its value for each case being consistent at 1σ . The corrective parameter f does not introduce significant improvements in the χ_{red}^2 value, and it is consistent with the values reported in Cao et al. (2012); Treu et al. (2006). When different sub-samples are used (e.g. SS2 to SS11), the cosmological parameter constraints are sensitive to the selected data (see figure 4, upper-right and middle panels). The ω_0 parameter prefers negative values leading to an accelerated expansion stage in all the scenarios excluding the $D^{obs} < 0.5$ region (SS2). The ω_1 parameter also adopt distinct values in all the cases. Like for w CDM and CPL models, we obtain large χ_{red}^2 values for the regions: $D^{obs} > 1$ (SS4), $\sigma < 210\text{ km s}^{-1}$ (SS5) and $\sigma > 276\text{ km s}^{-1}$ (SS8). Similarly, the best value for χ_{red}^2 is also achieved in the region $0.5 < D^{obs} < 1$ (SS3). The $D^{obs} < 0.5$ (SS2) region presents convergence problems as well, showing double contours in all the free parameters and being incompatible with an accelerated Universe. For the first three tests, the JBP constraints are inconsistent with those obtained by Wang et al. (2016) ($\omega_0 = -0.648 \pm 0.252$, $\omega_1 = -3.419 \pm 2.290$) and Magaña et al. (2017), ($\omega_0 = -0.80 \pm 0.45$, $\omega_1 = -3.78 \pm 3.73$). However, the constraint obtained for ω_0 in the region $0.5 \leq D^{obs} \leq 1$ is consistent with those estimated by Magaña et al. (2017) and Wang et al. (2016), although ω_1 is only consistent with the value obtained by Magaña et al. (2017). The FOM estimator gives tight constraints in the $0.5 \leq D^{obs} < 1$ (SS3) region and weak ones in $D^{obs} < 0.5$ (SS2) and $0.2 \leq z_i \leq 0.4$ (SS10) regions.

The figure 2 shows the reconstruction of the deceleration parameter for the JBP model using the constraints derived from each test. It is noticeable the $q(z)$ behavior showing a slowing down of the cosmic acceleration at late times for the SS3 and SS11. This behavior is in agreement with those found by several authors for these parametrizations (see for example Magaña et al. 2014; Wang et al. 2016). Notice also that SS2 and SS8 present a non standard behavior, i.e. they never cross the acceleration region. The remaining cases are in good agreement with the standard knowledge.

5.4 The impact of the f parameter

The mean values of the f parameter obtained with different models ($1.021_{-0.006}^{+0.012}$, $1.021_{-0.006}^{+0.008}$, and $1.021_{-0.006}^{+0.011}$ for ω CDM, CPL, and JBP respectively) are consistent with each other and also in agreement with those reported by Treu et al. (2006), and Cao et al. (2012). This indicates that the possible systematic errors affecting the image separation produced by the lens for our sample is estimated at most at 5 % when the value of f is considered equal for all SLS.

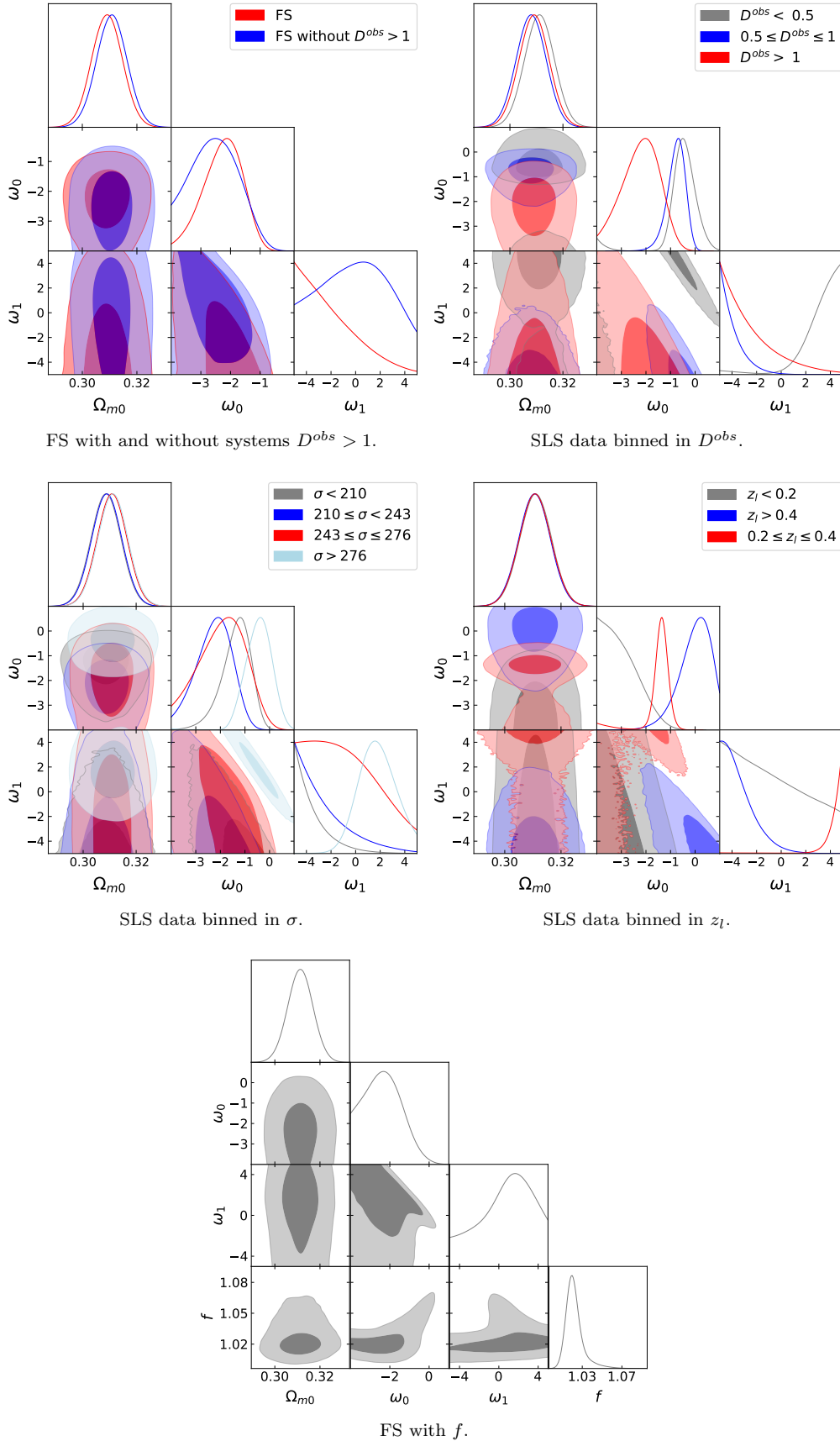


Figure 3. 1D marginalized posterior distributions and the 2D 68%, 99.7% confidence levels for the Ω_{m0} , ω_0 and ω_1 parameters of the CPL model and f parameter (lower panel) for the different samples presented in Table 2.

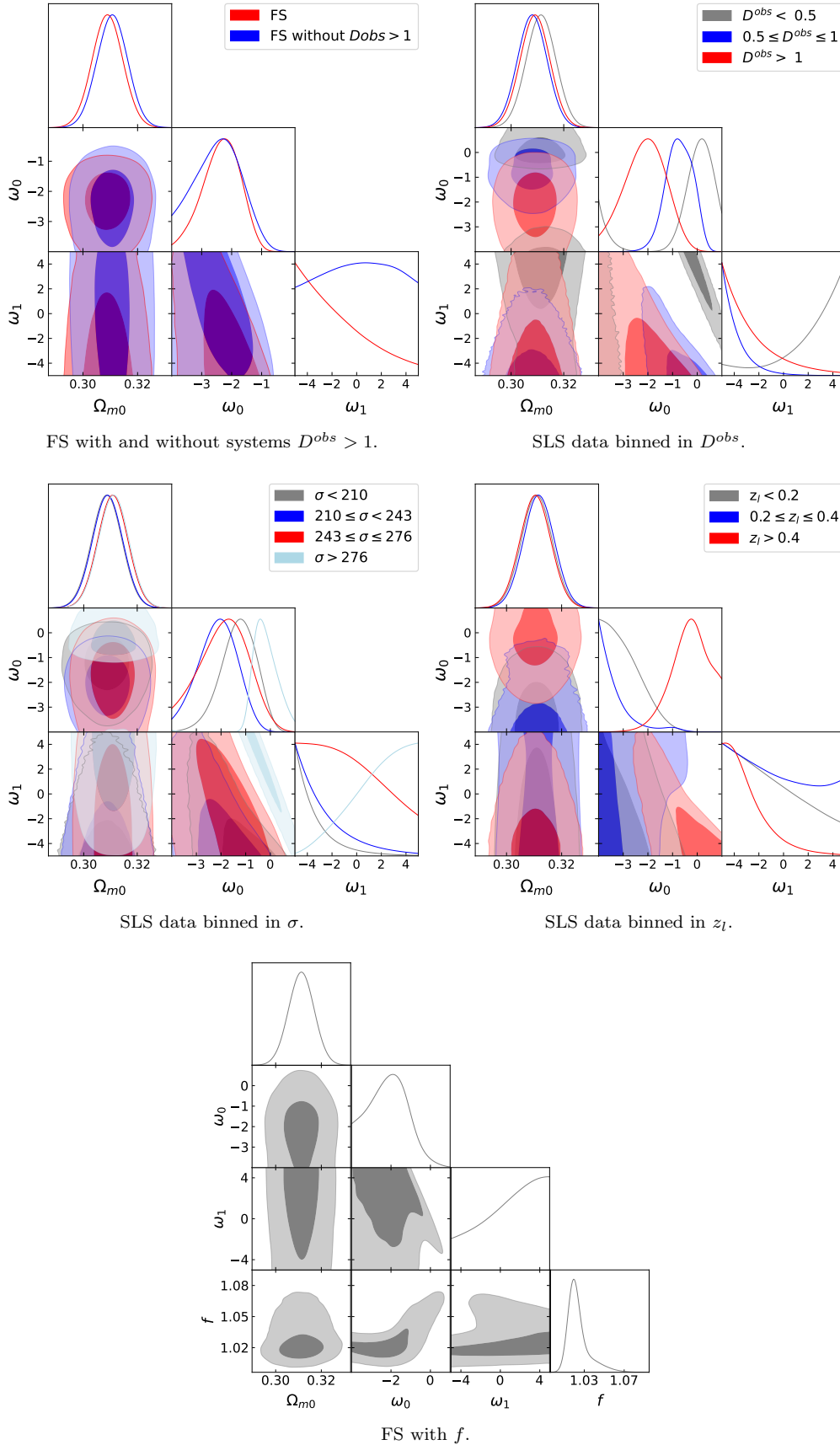


Figure 4. 1D marginalized posterior distributions and the 2D 68%, 99.7% confidence levels for the Ω_{m0} , ω_0 and ω_1 parameters of the JBP model and f parameter (lower panel) for the different samples presented in Table 2.

On the other hand, if we assume f as an independent free parameter in each SLS, the value of f becomes larger for some measured systems. However, if we restrict the analysis to the region between $0.5 \leq D^{obs} \leq 1$ (i.e., sample SS3) the scatter decreases (see Appendix B for details).

The deviation on the value of f could be related to the fact that some systems are not properly described by an isothermal model as found by Ritondale et al. (2018) for the BELLS gallery in almost all cases at the 2σ level. These deviations are also found by Barnabe et al. (2011), and by Vegetti et al. (2014) for the SLACS survey employing more sophisticated modelling. In this sense, in Appendix C we studied the effect of assuming a SIE (or a SIS) acting as a lens when the mass distribution follows a power-law. Although the scatter in f is even greater, with some systems outside the range proposed by Ofek et al. (2003), none of the mock systems shows a nonphysical value for D^{obs} . It is important to note that in most previous studies the lens models are close to isothermal. Thus, in this work we are using Eq. (4) as a first approximation, and Eq. (7) to take into account all the above mentioned irregularities (see for example Cao et al. 2012). Except those systematics that produces unphysically values on the observational lens equation.

5.5 The restricted sample SS3 as a fiduciary sample

Table 2 shows that there are four regions showing non-physical behaviours for the EoS of the dark energy (i.e. it does not satisfy $\omega_0 < -1/3$) or higher values for the χ^2_{min} function with respect to the FS, we label these sub-samples as unreliable (marked with a letter U in the table) since they have similar aspects among the cosmological models presented in this work being the following regions: SS2 ($D^{obs} < 0.5$) which present convergence problems in the estimation of cosmological parameters and a non-accelerating Universe at $z = 0$ for the ω CDM and JBP models, SS4 ($D^{obs} > 1$) showing a non physical value for the lens equation and the highest χ^2_{min} value for all the models, SS5 ($\sigma < 210 \text{ km s}^{-1}$) and SS8 ($\sigma > 276 \text{ km s}^{-1}$) showing higher χ^2_{min} values than those obtained for the FS and also showing a non-accelerating Universe in SS8 for the ω CDM model. It is worth to notice that the region SS11 ($D^{obs} \leq 1$ and $z_l > 0.4$) also presents a non-accelerating Universe at $z = 0$ for the CPL model, however is consistent with an accelerated one at 1σ of confidence level and do not show an increasing χ^2_{min} function in comparison with the FS, hence we do not discard this region from the following. Even though cosmological parameters has different mean values for the remaining samples, most are consistent at 1σ of confidence level for all the models.

However, to constrain cosmological parameters, we recommend the use of the restricted sample (SS3), which shows the best constraints and a lower dispersion in the value of the corrective parameter f , when is considered as an independent parameter in each SLS (see appendix B). The SS3 constraints for the different models, also shows consistency with CMB (Aghanim et al. 2018b) and SNe Ia (Scolnic et al. 2018) measurements. Therefore, we favour the SS3 sample as the fiduciary sample.

5.6 Comparing cosmological models

In this section, we discuss the comparison among cosmological models for only three samples: FS, FS+ f and SS3. We add to the present discussion the FS, FS+ f samples, because they are the complete samples (besides, as we appreciate in Table 2, χ^2_{red} values are very similar among the three models in them). Nevertheless, we highlight the results for the fiduciary SS3 sample.

In Table 3 we present the model selection's criteria, for the constraints obtained from the FS sample (with and without the f parameter), and the SS3 sample. To discern among models (in any sample), it is necessary to compare the different criterias; the favored model is obtained through the compromise between the AIC, BIC and FOM estimators. When we perform the model comparison using the FS constraints, the ω CDM model produce the lowest AIC and BIC values. By measuring the relative differences $\Delta AIC = AIC_i - AIC_{min}$, and $\Delta BIC = BIC_i - BIC_{min}$ (where the subindex i refers to the different models and AIC_{min} (BIC_{min}) is the lowest AIC (BIC) value) there is substantial support for the three models ($\Delta AIC < 2$ or ~ 2). However, exists positive evidence against the CPL and JBP models ($4.2 < \Delta BIC < 4.8$ respectively). By looking the FOM criteria, the highest values is obtained from the ω CDM model. Therefore, all estimators suggest that ω CDM is the favored model from the FS constraints. Similarly, the AIC, BIC, and FOM values from the FS+ f constraints suggest the same, the ω CDM model is the preferred one.

As mentioned before, we strongly suggest the use of SS3 sample to estimate cosmological parameters. In particular, for the constraints obtained for sample SS3, the lowest AIC and BIC values are obtained from the CPL model. Indeed, the relative difference ΔAIC with respect to this model (~ 3.1 and 6.2 for JBP and ω CDM model respectively) point out to a considerably less support for the these models. Moreover, the $\Delta BIC \sim 3.1$ and ~ 3.2 for the JBP and ω CDM model respectively, suggest a positive evidence against both models. By analyzing the FOM criteria, the highest value is obtained for the CPL model, i.e. it produce the strongest constraints. Thus, all the criteria suggest that the CPL is the favored model from the fiduciary SS3 sample. However, it is important to mention that does not exist enough evidence to rule out the ω CDM model. Therefore, when the SLS data are used as cosmological test in the range $0.5 \leq D^{obs} \leq 1$, a dynamical dark energy with a CPL parameterization is favored to explain the late cosmic acceleration.

6 CONCLUSIONS AND OUTLOOKS

In this paper we study three dark energy models: the ω CDM model with a DE constant equation of state, and the CPL and the JBP parametrizations where DE evolves with time. To constrain the cosmological parameters of the three models we used a new compilation of strong gravitational lens systems (SLS) with a total of 204 objects, the largest sample to date (details of all systems can be found in Appendix A1). We test the models using different cases. First considering all the systems using the D^{obs} estimated from the observed Einstein ring radius and velocity dispersion, secondly excluding those systems with a $D^{obs} > 1$ (unphysical)

Table 2. Mean values for the ω CDM, CPL and JBP parameters (Ω_{m0} , w_0 , w_1) and the f corrective parameter derived from different test employing the SLS data. We labeled some subsamples as U, which present weak constraints for all the models and unreliable results for the bayesian analysis.

Data set: data point number	χ^2_{min}	χ^2_{red}	Ω_{m0}	w_0	w_1	f
ω CDM model						
FS (all systems: 204)	570.359	2.824	$0.309^{+0.006}_{-0.006}$	$-2.478^{+0.479}_{-0.587}$	—	—
SS1 ($D^{obs} \leq 1$: 172)	409.759	2.396	$0.311^{+0.006}_{-0.006}$	$-2.593^{+0.794}_{-0.860}$	—	—
FS (all systems with f : 204)	559.619	2.784	$0.311^{+0.006}_{-0.006}$	$-2.013^{+1.229}_{-1.167}$	—	$1.021^{+0.012}_{-0.006}$
SS2 ($D^{obs} < 0.5$: 29) ^U	52.943	1.961	$0.312^{+0.006}_{-0.006}$	$0.572^{+0.174}_{-4.403}$	—	—
SS3 ($0.5 \leq D^{obs} \leq 1$: 143)	263.795	1.871	$0.308^{+0.006}_{-0.006}$	$-1.653^{+0.264}_{-0.322}$	—	—
SS4 ($D^{obs} > 1$: 32) ^U	383.875	2.258	$0.311^{+0.006}_{-0.006}$	$-2.336^{+0.684}_{-0.894}$	—	—
SS5 ($\sigma < 210 \text{ km s}^{-1}$: 64) ^U	201.766	3.254	$0.309^{+0.006}_{-0.006}$	$-2.100^{+0.416}_{-0.525}$	—	—
SS6 ($210 \text{ km s}^{-1} \leq \sigma < 243 \text{ km s}^{-1}$: 53)	118.092	2.316	$0.309^{+0.006}_{-0.006}$	$-2.633^{+0.550}_{-0.641}$	—	—
SS7 ($243 \text{ km s}^{-1} \leq \sigma \leq 276 \text{ km s}^{-1}$: 49)	107.252	2.282	$0.311^{+0.006}_{-0.006}$	$-1.854^{+0.672}_{-0.958}$	—	—
SS8 ($\sigma > 276 \text{ km s}^{-1}$: 38) ^U	109.457	3.040	$0.311^{+0.006}_{-0.006}$	$0.148^{+0.122}_{-0.134}$	—	—
SS9 ($D^{obs} \leq 1$ and $z_l < 0.2$: 52)	110.663	2.213	$0.311^{+0.006}_{-0.006}$	$-3.134^{+0.807}_{-0.603}$	—	—
SS10 ($D^{obs} \leq 1$ and $0.2 \leq z_l \leq 0.4$: 48)	112.860	2.453	$0.312^{+0.006}_{-0.006}$	$-3.558^{+0.701}_{-0.327}$	—	—
SS11 ($D^{obs} \leq 1$ and $z_l > 0.4$: 72)	149.099	2.129	$0.311^{+0.006}_{-0.006}$	$-1.163^{+0.318}_{-0.446}$	—	—
CPL model						
FS (all systems: 204)	569.317	2.832	$0.309^{+0.006}_{-0.006}$	$-2.224^{+0.612}_{-0.707}$	$-2.548^{+2.882}_{-1.765}$	—
SS1 ($D^{obs} \leq 1$: 172)	409.780	2.410	$0.311^{+0.006}_{-0.006}$	$-2.768^{+0.833}_{-0.764}$	$0.163^{+2.914}_{-3.270}$	—
FS (all systems with f : 204)	559.260	2.796	$0.311^{+0.006}_{-0.006}$	$-2.371^{+0.984}_{-0.984}$	$1.045^{+2.338}_{-3.219}$	$1.021^{+0.008}_{-0.006}$
SS2 ($D^{obs} < 0.5$: 29) ^U	46.235	1.778	$0.311^{+0.006}_{-0.006}$	$-0.505^{+0.456}_{-0.342}$	$3.585^{+0.989}_{-1.535}$	—
SS3 ($0.5 \leq D^{obs} \leq 1$: 143)	255.552	1.825	$0.308^{+0.006}_{-0.006}$	$-0.735^{+0.319}_{-0.395}$	$-4.202^{+1.208}_{-0.592}$	—
SS4 ($D^{obs} > 1$: 32) ^U	384.067	2.273	$0.311^{+0.006}_{-0.006}$	$-2.530^{+0.823}_{-0.832}$	$-0.056^{+2.871}_{-3.077}$	—
SS5 ($\sigma < 210 \text{ km s}^{-1}$: 64) ^U	196.854	3.227	$0.309^{+0.006}_{-0.006}$	$-1.292^{+0.500}_{-0.641}$	$-3.912^{+1.767}_{-2.813}$	—
SS6 ($210 \text{ km s}^{-1} \leq \sigma < 243 \text{ km s}^{-1}$: 53)	116.000	2.320	$0.309^{+0.006}_{-0.006}$	$-2.205^{+0.668}_{-0.789}$	$-3.159^{+2.728}_{-1.369}$	—
SS7 ($243 \text{ km s}^{-1} \leq \sigma \leq 276 \text{ km s}^{-1}$: 49)	107.363	2.334	$0.311^{+0.006}_{-0.006}$	$-1.856^{+0.889}_{-1.062}$	$-1.208^{+3.130}_{-2.580}$	—
SS8 ($\sigma > 276 \text{ km s}^{-1}$: 38) ^U	108.338	3.095	$0.311^{+0.006}_{-0.006}$	$-0.423^{+0.494}_{-0.552}$	$1.692^{+1.558}_{-1.438}$	—
SS9 ($D^{obs} \leq 1$ and $z_l < 0.2$: 52)	110.539	2.256	$0.311^{+0.006}_{-0.006}$	$-3.107^{+0.857}_{-0.624}$	$-1.148^{+3.690}_{-2.743}$	—
SS10 ($D^{obs} \leq 1$ and $0.2 \leq z_l \leq 0.4$: 48)	101.321	2.252	$0.311^{+0.006}_{-0.006}$	$-1.377^{+0.244}_{-0.284}$	$4.551^{+0.336}_{-0.781}$	—
SS11 ($D^{obs} \leq 1$ and $z_l > 0.4$: 72)	144.466	2.094	$0.311^{+0.006}_{-0.006}$	$0.049^{+0.536}_{-0.711}$	$-3.672^{+1.567}_{-0.925}$	—
JBP model						
FS (all systems: 204)	569.624	2.834	$0.309^{+0.006}_{-0.006}$	$-2.312^{+0.592}_{-0.671}$	$-2.220^{+3.368}_{-2.022}$	—
SS1 ($D^{obs} \leq 1$: 172)	409.750	2.410	$0.311^{+0.006}_{-0.006}$	$-2.671^{+0.801}_{-0.811}$	$0.201^{+3.209}_{-3.408}$	—
FS (all systems with f : 204)	559.147	2.796	$0.311^{+0.006}_{-0.006}$	$-2.124^{+0.960}_{-1.097}$	$1.367^{+2.544}_{-3.659}$	$1.021^{+0.011}_{-0.006}$
SS2 ($D^{obs} < 0.5$: 29) ^U	50.465	1.941	$0.311^{+0.006}_{-0.006}$	$-0.055^{+0.421}_{-0.396}$	$3.105^{+1.400}_{-3.034}$	—
SS3 ($0.5 \leq D^{obs} \leq 1$: 143)	258.744	1.848	$0.308^{+0.006}_{-0.006}$	$-1.047^{+0.324}_{-0.413}$	$-3.921^{+1.705}_{-0.805}$	—
SS4 ($D^{obs} > 1$: 32) ^U	383.931	2.272	$0.311^{+0.006}_{-0.006}$	$-2.433^{+0.754}_{-0.851}$	$0.125^{+3.203}_{-3.335}$	—
SS5 ($\sigma < 210 \text{ km s}^{-1}$: 64) ^U	198.932	3.261	$0.309^{+0.006}_{-0.006}$	$-1.617^{+0.502}_{-0.645}$	$-3.419^{+2.520}_{-1.181}$	—
SS6 ($210 \text{ km s}^{-1} \leq \sigma < 243 \text{ km s}^{-1}$: 53)	116.777	2.336	$0.309^{+0.006}_{-0.006}$	$-2.370^{+0.648}_{-0.742}$	$-2.682^{+3.262}_{-1.718}$	—
SS7 ($243 \text{ km s}^{-1} \leq \sigma \leq 276 \text{ km s}^{-1}$: 49)	107.317	2.333	$0.311^{+0.006}_{-0.006}$	$-1.869^{+0.821}_{-0.985}$	$-0.752^{+3.553}_{-2.911}$	—
SS8 ($\sigma > 276 \text{ km s}^{-1}$: 38) ^U	108.660	3.105	$0.311^{+0.006}_{-0.006}$	$-0.271^{+0.558}_{-0.404}$	$2.122^{+1.997}_{-2.838}$	—
SS9 ($D^{obs} \leq 1$ and $z_l < 0.2$: 52)	110.569	2.257	$0.311^{+0.006}_{-0.006}$	$-3.112^{+0.846}_{-0.619}$	$-1.012^{+3.686}_{-2.823}$	—
SS10 ($D^{obs} \leq 1$ and $0.2 \leq z_l \leq 0.4$: 48)	112.833	2.507	$0.311^{+0.006}_{-0.006}$	$-3.529^{+0.803}_{-0.349}$	$-0.663^{+3.849}_{-3.098}$	—
SS11 ($D^{obs} \leq 1$ and $z_l > 0.4$: 72)	147.010	2.131	$0.311^{+0.006}_{-0.006}$	$-0.589^{+0.510}_{-0.696}$	$-3.182^{+2.633}_{-1.341}$	—

Table 3. AIC, BIC and FOM values for the ω CDM, CPL and JBP models derived from different test employing the SLS data.

Data set	ω CDM			CPL			JBP		
	AIC	BIC	FOM	AIC	BIC	FOM	AIC	BIC	FOM
FS 204	574.359	580.995	343.671	575.317	585.271	143.0289	575.624	585.578	130.268
FS with f 204	565.619	575.573	18716.678	567.26	580.532	10122.341	567.147	580.419	7941.123
SS3 (143)	267.795	273.720	584.736	261.552	270.441	586.979	264.744	273.632	338.777

value, and finally using the entire sample with a new free parameter f that take into account systematics that might affect the observables. In addition, to assess the impact of some observables, we estimated the cosmological parameters using sub-samples of the SLS according to three different scenarios, considering distinct regions on the observational value of the lens equation (D^{obs}), the velocity dispersion (σ) and the redshift interval probed by the lens galaxy (z_l). We found weak constraints for some regions.

The f parameter is consistent among the three models (within 5% error), having similar values to those reported by Treu et al. (2006); Cao et al. (2012). Assuming f as an independent free parameter in each SLS, the cosmological constraints are consistent with those estimated assuming f equal for all the SLS. However, the scatter (in comparison with the Ofek estimations) of the value of f seems to be larger for some measured systems. To study this deviation, we analyze a mock catalog of 788 SLS, that mimics the distribution of the observational data compiled in this work. When the Einstein radius of the simulated sample is compared with the one obtained from a SIE fitting, we found that the error is less than 10% for most of the objects (see Appendix C). Considering that the majority of the data in our SLS compilation comes from models assuming SIEs, this supports the range of the parameter used in our paper. However, when a power-law mass distribution for the mock catalogue is assumed, the scatter of the Einstein radius increases (35% or less).

We found that some of the sub-samples considered in this work provide values for the cosmological parameters that are inconsistent with other observations (SNe Ia, CMB). Nevertheless, improvements on the constraints for all the models are reflected in the χ_{red}^2 value when we exclude the systems in the region of $D^{obs} > 1$. This unphysical region (also found by Leaf & Melia 2018) seems to be related to those systems with different kind of uncertainties (e.g. not fully confirmed lenses, multiple arcs, uncertain redshifts, complex lens substructure, see A2). Thus, as a byproduct of our analysis, results with $D^{obs} > 1$ point towards those systems with untrustworthy observed parameters or those which depart from our isothermal spherical mass distribution hypothesis (e.g. external shear and/or lens substructure). Most of the SLS considered in the present work have been modeled assuming a SIE lens model. Thus, the value of f obtained from the mock data deviates from the range proposed by Ofek et al. (2003) for some systems and a wider interval should be used.

Regarding the velocity dispersion, some of the selected regions provide weaker constraints (larger values in the χ_{red}^2 function): $\sigma < 210 \text{ km s}^{-1}$ and $\sigma > 276 \text{ km s}^{-1}$. Chen et al. (2018) also found weak constraints for the lens mass model parameters assuming different regions on the velocity dispersion. This could be due to an observational bias measuring the velocity dispersion σ , that can be related to a small θ_E , or not measuring the entire lens mass, or the lens galaxy has close companions.

We found that eight systems in the $D^{obs} < 0.5$ region can not be modeled properly by the theoretical lens equation, obtaining double confidence contours for the cosmological parameters. Finally, the lowest χ_{red}^2 value for each model is achieved in the $0.5 \leq D^{obs} \leq 1$ region, with values for the cosmological parameters ($-1.653 \leq \omega_0 \leq -0.735$

and $-4.202 \leq \omega_1 \leq -3.921$) in agreement with those expected from other astrophysical observations (see for instance (Magaña et al. 2014; Betoule et al. 2014; Aghanim et al. 2018b)). Therefore, we favour the SS3 sample as the fiduciary sample to constrain DE cosmological parameters. The model selection criteria show that the CPL model is preferred from this sample constraints, i.e. these data point out towards a dynamical dark energy behavior consistent with the three different criteria presented in table 3, obtaining $\omega_0 = -0.735^{+0.319}_{-0.395}$ and $\omega_1 = -4.202^{+1.208}_{-0.592}$ for this region. The estimation of the cosmological parameters presented in this paper, employing the strong lensing features of lens galaxies, provides constraints which are consistent with other cosmological probes (Magaña et al. 2014; Betoule et al. 2014; Scolnic et al. 2018; Magaña et al. 2017; Aghanim et al. 2018b). Nevertheless, a further analysis should be done, in particular to consider systematic biases, that help us to more tightly estimate cosmological parameters and improve our method.

ACKNOWLEDGMENTS

We thank the anonymous referee for thoughtful remarks and suggestions. Authors acknowledges the enlightening conversations and valuable feedback with Karina Rojas and Mario Rodriguez. M.H.A. acknowledges support from CONACYT PhD fellow, Consejo Zacatecano de Ciencia, Tecnología e Innovación (COZCYT) and Centro de Astrofísica de Valparaíso (CAV). M.H.A. thanks the staff of the Instituto de Física y Astronomía of the Universidad de Valparaíso where part of this work was done. J.M. acknowledges support from CONICYT project Basal AFB-170002 and CONICYT/FONDECYT 3160674. T.V. acknowledges support from PROGRAMA UNAM-DGAPA-PAPIIT IA102517. M.A.G.-A. acknowledges support from CONACYT research fellow, Sistema Nacional de Investigadores (SNI), COZCYT and Instituto Avanzado de Cosmología (IAC) collaborations. V.M. acknowledges support from Centro de Astrofísica de Valparaíso (CAV) and CONICYT REDES (190147).

DATA AVAILABILITY

The data underlying this article were accessed from the references presented in Table A1.

REFERENCES

- Abbott T. M. C., et al., 2019, *Astrophys. J.*, 872, L30
- Aghanim N., et al., 2018a
- Aghanim N., et al., 2018b
- Agnello A., et al., 2015, *MNRAS*, 454, 1260
- Akaike H., 1974, *IEEE Transactions on Automatic Control*, 19, 716
- Alam S., et al., 2017, *MNRAS*, 470, 2617
- Albrecht A., et al., 2006, *ArXiv Astrophysics e-prints*,
- Auger M. W., Treu T., Bolton A. S., Gavazzi R., Koopmans L. V. E., Marshall P. J., Bundy K., Moustakas L. A., 2009, *ApJ*, 705, 1099
- Barnabe M., Czoske O., Koopmans L. V. E., Treu T., Bolton A. S., 2011, *Mon. Not. Roy. Astron. Soc.*, 415, 2215

- Bautista J. E., et al., 2017, *A&A*, 603, A12
- Betoule M., et al., 2014, *Astronomy & Astrophysics*, 568, A22
- Biesiada M., 2006, *Phys. Rev.*, D73, 023006
- Biesiada M., Piórkowska A., Malec B., 2010, *MNRAS*, 406, 1055
- Bilic N., Tupper G. B., Viollier R. D., 2002, *Phys. Lett.*, B535, 17
- Blake C., et al., 2012, *MNRAS*, 425, 405
- Bolton A. S., Burles S., Koopmans L. V. E., Treu T., Moustakas L. A., 2006, *ApJ*, 638, 703
- Bolton A. S., Burles S., Koopmans L. V. E., Treu T., Gavazzi R., Moustakas L. A., Wayth R., Schlegel D. J., 2008, *Astrophys. J.*, 682, 964
- Brans C., Dicke R. H., 1961, *Phys. Rev.*, 124, 925
- Brownstein J. R., et al., 2012a, *ApJ*, 744, 41
- Brownstein J. R., et al., 2012b, *The Astrophysical Journal*, 744, 41
- Buchdahl H. A., 1970, *Monthly Notices of the Royal Astronomical Society*, 150, 1
- Cabanac R. A., et al., 2007, *A&A*, 461, 813
- Caldera-Cabral G., Maartens R., Ureña-López L. A., 2009, *Phys. Rev. D*, 79, 063518
- Caldwell R. R., 2002, *Phys. Lett.*, B545, 23
- Cao S., Pan Y., Biesiada M., Godlowski W., Zhu Z.-H., 2012, *J. Cosmology Astropart. Phys.*, 3, 016
- Cao S., Biesiada M., Gavazzi R., Pirkowska A., Zhu Z.-H., 2015, *Astrophys. J.*, 806, 185
- Cárdenas V. H., Rivera M., 2012, *Physics Letters B*, 710, 251
- Cárdenas V. H., Bernal C., Bonilla A., 2013, *MNRAS*, 433, 3534
- Chaplygin S., 1904, *Sci. Mem. Mosc. Univ. Math. Phys*, 21
- Chen Y., Li R., Shu Y., 2018
- Chevallier M., Polarski D., 2001, *Int. J. Mod. Phys.*, D10, 213
- Chiba T., Okabe T., Yamaguchi M., 2000, *Phys. Rev.*, D62, 023511
- Copeland E. J., Sami M., Tsujikawa S., 2006, *Int. J. Mod. Phys.*, D15, 1753
- Eisenstein D. J., et al., 2005, *ApJ*, 633, 560
- Foreman-Mackey D., Hogg D. W., Lang D., Goodman J., 2013, *Publ. Astron. Soc. Pac.*, 125, 306
- Futamase T., Yoshida S., 2001, *Prog. Theor. Phys.*, 105, 887
- Galiautdinov A., Kopeikin S. M., 2016, *Phys. Rev.*, D94, 044015
- García-Aspeitia M. A., Matos T., 2011, *Gen. Rel. Grav.*, 43, 315
- García-Aspeitia M. A., Magaña J., Hernández-Almada A., Motta V., 2018a, *International Journal of Modern Physics D*, 27, 1850006
- García-Aspeitia M. A., Hernández-Almada A., Magaña J., Amante M. H., Motta V., Martínez-Robles C., 2018b, *Phys. Rev.*, D97, 101301
- García-Aspeitia M. A., Martínez-Robles C., Hernández-Almada A., Magaña J., Motta V., 2019, *Phys. Rev.*, D99, 123525
- Gelman A., Rubin D. B., 1992, *Statist. Sci.*, 7, 457
- Grillo C., Lombardi M., Bertin G., 2008, *A&A*, 477, 397
- Hernandez-Almada A., Magana J., Garcia-Aspeitia M. A., Motta V., 2018
- Hewett P. C., Irwin M. J., Foltz C. B., Harding M. E., Corrigan R. T., Webster R. L., Dinshaw N., 1994, *AJ*, 108, 1534
- Inada N., et al., 2003, *AJ*, 126, 666
- Inada N., et al., 2005, *AJ*, 130, 1967
- Jassal H. K., Bagla J. S., Padmanabhan T., 2005, *Mon. Not. Roy. Astron. Soc.*, 356, L11
- Jimenez R., Loeb A., 2002, *Astrophys. J.*, 573, 37
- Jorgensen I., Franx M., Kjaergaard P., 1995a, *MNRAS*, 273, 1097
- Jorgensen I., Franx M., Kjaergaard P., 1995b, *MNRAS*, 276, 1341
- Jullo E., Natarajan P., Kneib J. P., D'Aloisio A., Limousin M., Richard J., Schimd C., 2010, *Science*, 329, 924
- Kamenshchik A. Yu., Moschella U., Pasquier V., 2001, *Phys. Lett.*, B511, 265
- Keeton C. R., 2011, *GRAVLENS: Computational Methods for Gravitational Lensing* (ascl:1102.003)
- Kochanek C. S., 1995, *ApJ*, 445, 559
- Koopmans L. V. E., Treu T., 2003a, *ApJ*, 583, 606
- Koopmans L. V. E., Treu T., 2003b, *Astrophys. J.*, 583, 606
- Lacy M., Gregg M., Becker R. H., White R. L., Glikman E., Helfand D., Winn J. N., 2002, *AJ*, 123, 2925
- Langlois D., Saito R., Yamauchi D., Noui K., 2018, *Phys. Rev.*, D97, 061501
- Leaf K., Melia F., 2018, *Mon. Not. Roy. Astron. Soc.*, 478, 5104
- Lehar J., Cooke A. J., Lawrence C. R., Silber A. D., Langston G. I., 1996, *AJ*, 111, 1812
- Leier D., Ferreras I., Saha P., Falco E. E., 2011, *ApJ*, 740, 97
- Li M., Li X.-D., Wang S., Wang Y., 2011, *Communications in Theoretical Physics*, 56, 525
- Linder E. V., 2003, *Phys. Rev.*, D68, 083503
- Magaña J., Cárdenas V. H., Motta V., 2014, *J. Cosmology Astropart. Phys.*, 10, 017
- Magaña J., Motta V., Cárdenas V. H., Verdugo T., Jullo E., 2015, *ApJ*, 813, 69
- Magaña J., Motta V., Cardenas V. H., Foex G., 2017, *Mon. Not. Roy. Astron. Soc.*, 469, 47
- Magaña J., Acebrón A., Motta V., Verdugo T., Jullo E., Limousin M., 2018, *ApJ*, 865, 122
- Magaña J., Amante M. H., Garcia-Aspeitia M. A., Motta V., 2018, *Mon. Not. Roy. Astron. Soc.*, 476, 1036
- Melia F., Wei J.-J., Wu X.-F., 2015, *Astron. J.*, 149, 2
- Moresco M., et al., 2016, *Journal of Cosmology and Astro-Particle Physics*, 2016, 014
- Morgan N. D., Becker R. H., Gregg M. D., Schechter P. L., White R. L., 2001, *Astron. J.*, 121, 611
- Morgan N. D., Kochanek C. S., Pevunova O., Schechter P. L., 2005, *AJ*, 129, 2531
- Muñoz J. A., Falco E. E., Kochanek C. S., Lehár J., McLeod B. A., Impey C. D., Rix H.-W., Peng C. Y., 1998, *Ap&SS*, 263, 51
- Muñoz J. A., Kochanek C. S., Keeton C. R., 2001, *ApJ*, 558, 657
- Ofek E. O., Rix H.-W., Maoz D., 2003, *Mon. Not. Roy. Astron. Soc.*, 343, 639
- Ofek E. O., Maoz D., Rix H.-W., Kochanek C. S., Falco E. E., 2006, *ApJ*, 641, 70
- Perez A., Sudarsky D., 2017
- Perlmutter S., Aldering G., Goldhaber G., Knop R. A., Nugent P., others Project T. S. C., 1999, *The Astrophysical Journal*, 517, 565
- Pindor B., et al., 2004, *AJ*, 127, 1318
- Planck Collaboration et al., 2016, *A&A*, 594, A13
- Qi J.-Z., Cao S., Zhang S., Biesiada M., Wu Y., Zhu Z.-H., 2018, preprint, (arXiv:1803.01990)
- Ratra B., Peebles P. J. E., 1988, *Phys. Rev. D*, 37, 3406
- Riess A. G., Filippenko A. V., Challis P., Clocchiatti A., Diercks A., et al., 1998, *The Astronomical Journal*, 116, 1009
- Riess A. G., et al., 2016, *Astrophys. J.*, 826, 56
- Riess A. G., Casertano S., Yuan W., Macri L. M., Scolnic D., 2019, arXiv e-prints,
- Ritondale E., Auger M. W., Vegetti S., McKean J. P., 2018, *Monthly Notices of the Royal Astronomical Society*, 482, 4744
- Rusin D., Norbury M., Biggs A. D., Marlow D. R., Jackson N. J., Browne I. W. A., Wilkinson P. N., Myers S. T., 2002, *MNRAS*, 330, 205
- Rusin D., et al., 2003a, *ApJ*, 587, 143
- Rusin D., Kochanek C. S., Keeton C. R., 2003b, *ApJ*, 595, 29
- Schmidt B. P., Suntzeff N. B., Phillips M. M., Schommer R. A., Clocchiatti A., et al., 1998, *The Astrophysical Journal*, 507, 46
- Schneider P., Ehlers J., Falco E. E., 1992, *Gravitational Lenses*, doi:10.1007/978-3-662-03758-4.
- Schwarz G., 1978, *Annals of Statistics*, 6, 461
- Scolnic D. M., et al., 2018, *Astrophys. J.*, 859, 101

- Shi K., Huang Y., Lu T., 2012, *Mon. Not. Roy. Astron. Soc.*, 426, 2452
- Shu Y., et al., 2016, *The Astrophysical Journal*, 833, 264
- Shu Y., et al., 2017, *ApJ*, 851, 48
- Sonnenfeld A., Gavazzi R., Suyu S. H., Treu T., Marshall P. J., 2013a, *Astrophys. J.*, 777, 97
- Sonnenfeld A., Treu T., Gavazzi R., Suyu S. H., Marshall P. J., Auger M. W., Nipoti C., 2013b, *Astrophys. J.*, 777, 98
- Sonnenfeld A., Treu T., Marshall P. J., Suyu S. H., Gavazzi R., Auger M., Nipoti C., 2015, *Astrophys. J.*, 800, 94
- Sotiriou T. P., Faraoni V., 2010, *Rev. Mod. Phys.*, 82, 451
- Spingola C., McKean J. P., Auger M. W., Fassnacht C. D., Koopmans L. V. E., Lagattuta D. J., Vegetti S., 2018, *MNRAS*, 478, 4816
- Starobinsky A., 1980, *Physics Letters B*, 91, 99
- Tonry J. L., 1998, *AJ*, 115, 1
- Treu T., Koopmans L., 2002, *Astrophys. J.*, 575, 87
- Treu T., Koopmans L. V. E., 2004, *ApJ*, 611, 739
- Treu T., Koopmans L. V., Bolton A. S., Burles S., Moustakas L. A., 2006, *ApJ*, 640, 662
- Treu T., et al., 2018, *MNRAS*, 481, 1041
- Turner E. L., Ostriker J. P., Gott J. R. I., 1984, *ApJ*, 284, 1
- Vegetti S., Koopmans L. V. E., Auger M. W., Treu T., Bolton A. S., 2014, *Mon. Not. Roy. Astron. Soc.*, 442, 2017
- Wang Y., 2008, *Phys. Rev. D*, 77, 123525
- Wang S., Hu Y., Li M., Li N., 2016, *ApJ*, 821, 60
- Weinberg S., 1989, *Reviews of Modern Physics*, 61
- Wetterich C., 1988, *Nuclear Physics B*, 302, 668
- Yennapureddy M. K., Melia F., 2018, *Eur. Phys. J.*, C78, 258
- Zeldovich Y. B., 1968, *Soviet Physics Uspekhi*, 11
- Zhang M.-J., Xia J.-Q., 2018, *Nuclear Physics B*, 929, 438

APPENDIX A: STRONG-LENSING SYSTEMS COMPILATION

- In Table A1 presents the compilation of SLS with 204 points.

- Table A2 shows the 32 systems with $D^{obs} > 1$. Many of these systems appear flagged, which means that such objects are: not confirmed lenses, or have complex source structures with multiple arcs and counter-arcs, or the foreground lens is clearly composed of two distinct components, have uncertain redshift measurements, or the arcs (rings) are embedded in the light of the foreground lens. We refer the interested reader to the references presented in Table A1. We suggest that these systems with $D^{obs} > 1$, should not be used in cosmological parameter estimation (see also Leaf & Melia 2018).

APPENDIX B: THE EFFECT OF f AS AN INDIVIDUAL AND FREE PARAMETER FOR EACH SLS MEASUREMENT

In the third test (FS with f) presented in Table 2, we estimated cosmological parameters under the hypothesis that all the measurements has the same value for the f parameter in Eq. (7). This corrective parameter, has been introduced to explain unknown systematics that can be produced by some of the assumptions mentioned in section 2. However, each SLS has been study under different circumstances and employing different telescopes and instruments. Therefore, the unknown systematics should not be the same, i.e

the value for the corrective parameter f must be different in each case. To quantify this, we carried out an optimization for the parameters considering f as an individual and free parameter for each SLS. We performed the optimization for the ω CDM model through the differential evolution method from *scipy* python package. We assume the same priors for the ω ($-4 < \omega < 1$) and Ω_{m0} (gaussian prior of $\Omega_{m0} = 0.3111 \pm 0.0056$) parameters, nevertheless, to assess the impact of the possible systematic errors, we consider a bigger interval for the f parameter within the following range $0.6 < f < 1.5$.

Figure B1 shows the histogram of the values obtained for the f parameter when the complete and SS3 sample ($0.5 \leq D^{obs} \leq 1$) are considered. For the complete sample, this result show that many systems are outside of the region proposed by Treu et al. (2006), and Ofek et al. (2003). In particular nine systems have extreme f values, eight with $f = 1.5$ and one at $f = 0.6$. Which suggests that some measured systems have larger systematic errors. However, when we use the SS3 sample, only one system take a value of $f = 1.5$ and the remain systems that are beyond the mentioned region are considerably less. This result indicates that the corrective parameter f decreases when the SS3 sample is considered, and it is consistent with the results obtained for the three cosmological models, obtaining the lowest values for χ_{red}^2 (see table 2). Nevertheless, the two samples have similar f mean values, obtaining $f = 1.10$ and $f = 1.09$ for the complete and SS3 sample respectively. Following the same procedure, we optimize the cosmological parameters for the CPL, and JBP models along with f (as individual free parameter in each SLS). Obtaining the same behavior as in the ω CDM scenario for both samples. Therefore, under the assumption that each SLS has its own associated f , we do not expect significant differences in the cosmological constraints. Indeed, in Figures B2-B4 we show the histograms of the cosmological parameter best fits when f takes different values in each data point on the FS sample. To compare with the MCMC analysis of section 5, we fit a Gaussian kernel to these histograms and calculate the mean values and their uncertainties. We obtain for the w CDM model $w_0 = -1.62_{-1.28}^{+1.31}$. This result is consistent with the value reported in Table 2 (FS+ f) within $\sim 1.02\sigma$. For the optimization in the CPL model, we obtain the constraints $w_0 = -1.99_{-1.25}^{+1.80}$ and $w_1 = -0.10_{-3.50}^{+2.91}$, which are also consistent with the MCMC results within $\sim 0.83\sigma$, and $\sim 0.32\sigma$ respectively. Similarly, for the JBP model, the individual optimization gives $w_0 = -2.07_{-1.03}^{+1.69}$, and $w_1 = -0.53_{-3.40}^{+3.82}$. These values are in agreement within $\sim 0.58\sigma$, and $\sim 0.43\sigma$, with the values reported in Table 2.

APPENDIX C: MOCK DATA WITH STRONG-LENSING SYSTEMS

In this section, we use a mock data set of SLS to estimate the effect on the f parameter when we use the θ_E values reported in the literature.

To simulate our data we procede as follow: mimicking the same distribution of z_s of our SLS sample (within the range $0.196 < z_s < 3.595$), we generate an aleatory sample of 1000 sources. Then, for each source we calculate the most probably redshift of the lens, z_l , following the work of Turner

Table A1. Compilation of 204 strong-lensing measurements. Here, the * indicates that the uncertainties were estimated.

System Name	Survey	z_l	z_s	$\theta_E(\prime)$	σ_0 (Km s $^{-1}$)	Reference
SDSSJ0819+4534	SLACS	0.194	0.446	0.85	225 \pm 15	Auger et al. (2009)
SDSSJ0959+4416	SLACS	0.237	0.531	0.96	244 \pm 19	Bolton et al. (2008)
SDSSJ1029+0420	SLACS	0.104	0.615	1.01	210 \pm 11	Bolton et al. (2008)
SDSSJ1103+5322	SLACS	0.158	0.735	1.02	196 \pm 12	Bolton et al. (2008)
SDSSJ1306+0600	SLACS	0.173	0.472	1.32	237 \pm 17	Auger et al. (2009)
SDSSJ1313+4615	SLACS	0.185	0.514	1.37	221 \pm 17	Auger et al. (2009)
SDSSJ1318-0313	SLACS	0.240	1.300	1.58	213 \pm 18	Auger et al. (2009)
SDSSJ1420+6019	SLACS	0.063	0.535	1.04	205 \pm 10	Bolton et al. (2008)
SDSSJ1443+0304	SLACS	0.134	0.419	0.81	209 \pm 11	Bolton et al. (2008)
SDSSJ1614+4522	SLACS	0.178	0.811	0.84	182 \pm 13	Bolton et al. (2008)
SDSSJ1644+2625	SLACS	0.137	0.610	1.27	229 \pm 12	Auger et al. (2009)
SDSSJ1719+2939	SLACS	0.181	0.578	1.28	286 \pm 15	Auger et al. (2009)
HE0047-1756	CASTLES	0.408	1.670	0.80	190 \pm 27*	Ofek et al. (2006)
HE0230-2130	CASTLES	0.522	2.162	0.87	240 \pm 34*	Ofek et al. (2006)
J0246-0825	CASTLES	0.723	1.686	0.53	265 \pm 37*	Inada et al. (2005)
HE0435-1223	CASTLES	0.454	1.689	1.22	257 \pm 36*	Morgan et al. (2005)
SDSSJ092455.87+021924.9	CASTLES	0.393	1.523	0.88	230 \pm 32*	Inada et al. (2003)
LBQS1009-0252	CASTLES	0.871	2.739	0.77	245 \pm 34*	Hewett et al. (1994)
J1004+1229	CASTLES	0.950	2.640	0.83	240 \pm 34*	Lacy et al. (2002)
SDSSJ115517.35+634622.0	CASTLES	0.176	2.888	0.76	190 \pm 27*	Pindor et al. (2004)
FBQ1633+3134	CASTLES	0.684	1.518	0.35	160 \pm 22*	Morgan et al. (2001)
MG1654+1346	CASTLES	0.254	1.740	1.05	200 $^{+120}_{-80}$	Rusin et al. (2003a)
DES J2146-0047	DES	0.799	2.38	0.68	215 \pm 21*	Agnello et al. (2015)
SDSSJ0151+0049	BELLS	0.517	1.364	0.68	219 \pm 39	Brownstein et al. (2012b)
SDSSJ0747+5055	BELLS	0.438	0.898	0.75	328 \pm 60	Brownstein et al. (2012b)
SDSSJ0747+4448	BELLS	0.437	0.897	0.61	281 \pm 52	Brownstein et al. (2012b)
SDSSJ0801+4727	BELLS	0.483	1.518	0.49	98 \pm 24	Brownstein et al. (2012b)
SDSSJ0830+5116	BELLS	0.53	1.332	1.14	268 \pm 36	Brownstein et al. (2012b)
SDSSJ0944-0147	BELLS	0.539	1.179	0.72	204 \pm 34	Brownstein et al. (2012b)
SDSSJ1159-0007	BELLS	0.579	1.346	0.68	165 \pm 41	Brownstein et al. (2012b)
SDSSJ1215+0047	BELLS	0.642	1.297	1.37	262 \pm 45	Brownstein et al. (2012b)
SDSSJ1221+3806	BELLS	0.535	1.284	0.7	187 \pm 48	Brownstein et al. (2012b)
SDSSJ1234-0241	BELLS	0.49	1.016	0.53	122 \pm 31	Brownstein et al. (2012b)
SDSSJ1318-0104	BELLS	0.659	1.396	0.68	177 \pm 27	Brownstein et al. (2012b)
SDSSJ1337+3620	BELLS	0.564	1.182	1.39	225 \pm 35	Brownstein et al. (2012b)
SDSSJ1349+3612	BELLS	0.44	0.893	0.75	178 \pm 18	Brownstein et al. (2012b)
SDSSJ1352+3216	BELLS	0.463	1.034	1.82	161 \pm 21	Brownstein et al. (2012b)
SDSSJ1522+2910	BELLS	0.555	1.311	0.74	166 \pm 27	Brownstein et al. (2012b)
SDSSJ1541+1812	BELLS	0.56	1.113	0.64	174 \pm 24	Brownstein et al. (2012b)
SDSSJ1542+1629	BELLS	0.352	1.023	1.04	210 \pm 16	Brownstein et al. (2012b)
SDSSJ1545+2748	BELLS	0.522	1.289	1.21	250 \pm 37	Brownstein et al. (2012b)
SDSSJ1601+2138	BELLS	0.544	1.446	0.86	207 \pm 36	Brownstein et al. (2012b)
SDSSJ1631+1854	BELLS	0.408	1.086	1.63	272 \pm 14	Brownstein et al. (2012b)
SDSSJ2122+0409	BELLS	0.626	1.452	1.58	324 \pm 56	Brownstein et al. (2012b)
SDSSJ2125+0411	BELLS	0.363	0.978	1.2	247 \pm 17	Brownstein et al. (2012b)
SDSSJ2303+0037	BELLS	0.458	0.936	1.02	274 \pm 31	Brownstein et al. (2012b)
SDSSJ0008-0004	SLACS	0.44	1.192	1.16	193 \pm 36	Auger et al. (2009)
SDSSJ0029-0055	SLACS	0.227	0.931	0.96	229 \pm 18	Auger et al. (2009)
SDSSJ0037-0942	SLACS	0.196	0.632	1.53	279 \pm 10	Auger et al. (2009)
SDSSJ0044+0113	SLACS	0.12	0.196	0.79	266 \pm 13	Auger et al. (2009)
SDSSJ0109+1500	SLACS	0.294	0.525	0.69	251 \pm 19	Auger et al. (2009)
SDSSJ0157-0056	SLACS	0.513	0.924	0.79	295 \pm 47	Auger et al. (2009)
SDSSJ0216-0813	SLACS	0.332	0.524	1.16	333 \pm 23	Auger et al. (2009)
SDSSJ0252+0039	SLACS	0.28	0.982	1.04	164 \pm 12	Auger et al. (2009)
SDSSJ0330-0020	SLACS	0.351	1.071	1.1	212 \pm 21	Auger et al. (2009)
SDSSJ0405-0455	SLACS	0.075	0.81	0.8	160 \pm 7	Auger et al. (2009)
SDSSJ0728+3835	SLACS	0.206	0.688	1.25	214 \pm 11	Auger et al. (2009)
SDSSJ0737+3216	SLACS	0.322	0.581	1	338 \pm 16	Auger et al. (2009)
SDSSJ0808+4706	SLACS	0.219	1.025	1.23	236 \pm 11	Auger et al. (2009)
SDSSJ0822+2652	SLACS	0.241	0.594	1.17	259 \pm 15	Auger et al. (2009)
SDSSJ0841+3824	SLACS	0.116	0.657	1.41	225 \pm 8	Auger et al. (2009)
SDSSJ0903+4116	SLACS	0.43	1.065	1.29	223 \pm 27	Auger et al. (2009)
SDSSJ0912+0029	SLACS	0.164	0.324	1.63	326 \pm 12	Auger et al. (2009)

Table A1 – *continued*

System Name	Survey	z_l	z_s	$\theta_E(\prime)$	σ_0 (Km s ⁻¹)	Reference
SDSSJ0936+0913	SLACS	0.19	0.588	1.09	243 ±11	Auger et al. (2009)
SDSSJ0946+1006	SLACS	0.222	0.608	1.38	263 ±21	Auger et al. (2009)
SDSSJ0956+5100	SLACS	0.24	0.47	1.33	334 ±15	Auger et al. (2009)
SDSSJ0959+0410	SLACS	0.126	0.535	0.99	197 ±13	Auger et al. (2009)
SDSSJ1016+3859	SLACS	0.168	0.439	1.09	247 ±13	Auger et al. (2009)
SDSSJ1020+1122	SLACS	0.282	0.553	1.2	282 ±18	Auger et al. (2009)
SDSSJ1023+4230	SLACS	0.191	0.696	1.41	242 ±15	Auger et al. (2009)
SDSSJ1100+5329	SLACS	0.317	0.858	1.52	187 ±23	Auger et al. (2009)
SDSSJ1106+5228	SLACS	0.096	0.407	1.23	262 ±9	Auger et al. (2009)
SDSSJ1112+0826	SLACS	0.273	0.63	1.49	320 ±20	Auger et al. (2009)
SDSSJ1134+6027	SLACS	0.153	0.474	1.1	239 ±11	Auger et al. (2009)
SDSSJ1142+1001	SLACS	0.222	0.504	0.98	221 ±22	Auger et al. (2009)
SDSSJ1143-0144	SLACS	0.106	0.402	1.68	269 ±5	Auger et al. (2009)
SDSSJ1153+4612	SLACS	0.18	0.875	1.05	269 ±15	Auger et al. (2009)
SDSSJ1204+0358	SLACS	0.164	0.631	1.31	267 ±17	Auger et al. (2009)
SDSSJ1205+4910	SLACS	0.215	0.481	1.22	281 ±13	Auger et al. (2009)
SDSSJ1213+6708	SLACS	0.123	0.64	1.42	292 ±11	Auger et al. (2009)
SDSSJ1218+0830	SLACS	0.135	0.717	1.45	219 ±10	Auger et al. (2009)
SDSSJ1250+0523	SLACS	0.232	0.795	1.13	252 ±14	Auger et al. (2009)
SDSSJ1330-0148	SLACS	0.081	0.712	0.87	185 ±9	Auger et al. (2009)
SDSSJ1402+6321	SLACS	0.205	0.481	1.35	267 ±17	Auger et al. (2009)
SDSSJ1403+0006	SLACS	0.189	0.473	0.83	213 ±17	Auger et al. (2009)
SDSSJ1416+5136	SLACS	0.299	0.811	1.37	240 ±25	Auger et al. (2009)
SDSSJ1430+4105	SLACS	0.285	0.575	1.52	322 ±32	Auger et al. (2009)
SDSSJ1436-0000	SLACS	0.285	0.805	1.12	281 ±19	Auger et al. (2009)
SDSSJ1451-0239	SLACS	0.125	0.52	1.04	223 ±14	Auger et al. (2009)
SDSSJ1525+3327	SLACS	0.358	0.717	1.31	264 ±26	Auger et al. (2009)
SDSSJ1531-0105	SLACS	0.16	0.744	1.71	279 ±12	Auger et al. (2009)
SDSSJ1538+5817	SLACS	0.143	0.531	1	189 ±12	Auger et al. (2009)
SDSSJ1621+3931	SLACS	0.245	0.602	1.29	236 ±20	Auger et al. (2009)
SDSSJ1627-0053	SLACS	0.208	0.524	1.23	290 ±14	Auger et al. (2009)
SDSSJ1630+4520	SLACS	0.248	0.793	1.78	276 ±16	Auger et al. (2009)
SDSSJ1636+4707	SLACS	0.228	0.674	1.09	231 ±15	Auger et al. (2009)
SDSSJ2238-0754	SLACS	0.137	0.713	1.27	198 ±11	Auger et al. (2009)
SDSSJ2300+0022	SLACS	0.228	0.464	1.24	279 ±17	Auger et al. (2009)
SDSSJ2303+1422	SLACS	0.155	0.517	1.62	255 ±16	Auger et al. (2009)
SDSSJ2321-0939	SLACS	0.082	0.532	1.6	249 ±8	Auger et al. (2009)
SDSSJ2341+0000	SLACS	0.186	0.807	1.44	207 ±13	Auger et al. (2009)
Q0047-2808	LSD	0.485	3.595	1.34 ±0.01	229 ±15	Koopmans & Treu (2003b)
CFRS03-1077	LSD	0.938	2.941	1.24 ±0.06	251 ±19	Treu & Koopmans (2004)
HST14176+5226	LSD	0.81	3.399	1.41 ±0.08	224 ±15	Treu & Koopmans (2004)
HST15433	LSD	0.497	2.092	0.36 ±0.04	116 ±10	Treu & Koopmans (2004)
SL2SJ021247-055552	SL2S	0.75	2.74	1.27 ±0.04	273 ±22	Sonnenfeld et al. (2013b)
SL2SJ021325-074355	SL2S	0.717	3.48	2.39 ±0.07	293 ±34	Sonnenfeld et al. (2013b)
SL2SJ021411-040502	SL2S	0.609	1.88	1.41 ±0.04	287 ±47	Sonnenfeld et al. (2013b)
SL2SJ021737-051329	SL2S	0.646	1.847	1.27 ±0.04	239 ±27	Sonnenfeld et al. (2013b)
SL2SJ021902-082934	SL2S	0.389	2.15	1.30 ±0.04	289 ±23	Sonnenfeld et al. (2013b)
SL2SJ022346-053418	SL2S	0.499	1.44	1.22 ±0.11	288 ±28	Sonnenfeld et al. (2013b)
SL2SJ022511-045433	SL2S	0.238	1.199	1.76 ±0.05	234 ±21	Sonnenfeld et al. (2013b)
SL2SJ022610-042011	SL2S	0.494	1.232	1.19 ±0.04	263 ±24	Sonnenfeld et al. (2013b)
SL2SJ023251-040823	SL2S	0.352	2.34	1.04 ±0.03	281 ±26	Sonnenfeld et al. (2013b)
SL2SJ084847-035103	SL2S	0.682	1.55	0.85 ±0.07	197 ±21	Sonnenfeld et al. (2013b)
SL2SJ084909-041226	SL2S	0.722	1.54	1.10 ±0.03	320 ±24	Sonnenfeld et al. (2013b)
SL2SJ084959-025142	SL2S	0.274	2.09	1.16 ±0.04	276 ±35	Sonnenfeld et al. (2013b)
SL2SJ085019-034710	SL2S	0.337	3.25	0.93 ±0.03	290 ±24	Sonnenfeld et al. (2013b)
SL2SJ085540-014730	SL2S	0.365	3.39	1.03 ±0.04	222 ±25	Sonnenfeld et al. (2013b)
SL2SJ085559-040917	SL2S	0.419	2.95	1.36 ±0.10	281 ±22	Sonnenfeld et al. (2013b)
SL2SJ090407-005952	SL2S	0.611	2.36	1.40 ±0.04	183 ±21	Sonnenfeld et al. (2013b)
SL2SJ095921+020638	SL2S	0.552	3.35	0.74 ±0.02	188 ±22	Sonnenfeld et al. (2013b)
SL2SJ135949+553550	SL2S	0.783	2.77	1.14 ±0.03	228 ±29	Sonnenfeld et al. (2013b)
SL2SJ140454+520024	SL2S	0.456	1.59	2.55 ±0.08	342 ±20	Sonnenfeld et al. (2013b)
SL2SJ140546+524311	SL2S	0.526	3.01	1.51 ±0.05	284 ±21	Sonnenfeld et al. (2013b)
SL2SJ140650+522619	SL2S	0.716	1.47	0.94 ±0.03	253 ±19	Sonnenfeld et al. (2013b)
SL2SJ141137+565119	SL2S	0.322	1.42	0.93 ±0.03	214 ±23	Sonnenfeld et al. (2013b)
SL2SJ142031+525822	SL2S	0.38	0.99	0.96 ±0.14	246 ±23	Sonnenfeld et al. (2013b)
SL2SJ142059+563007	SL2S	0.483	3.12	1.40 ±0.04	228 ±19	Sonnenfeld et al. (2013b)

Table A1 – *continued*

System Name	Survey	z_l	z_s	$\theta_E(\prime)$	σ_0 (Km s $^{-1}$)	Reference
SL2SJ220329+020518	SL2S	0.4	2.15	1.95 \pm 0.06	213 \pm 21	Sonnenfeld et al. (2013b)
SL2SJ220506+014703	SL2S	0.476	2.53	1.66 \pm 0.06	317 \pm 30	Sonnenfeld et al. (2013b)
SL2SJ221326–000946	SL2S	0.338	3.45	1.07 \pm 0.03	165 \pm 20	Sonnenfeld et al. (2013b)
SL2SJ221929–001743	SL2S	0.289	1.02	0.52 \pm 0.13	189 \pm 20	Sonnenfeld et al. (2013b)
SL2SJ222012+010606	SL2S	0.232	1.07	2.16 \pm 0.07	127 \pm 15	Sonnenfeld et al. (2013b)
SL2SJ222148+011542	SL2S	0.325	2.35	1.40 \pm 0.05	222 \pm 23	Sonnenfeld et al. (2013b)
SL2SJ222217+001202	SL2S	0.436	1.36	1.44 \pm 0.15	221 \pm 22	Sonnenfeld et al. (2013b)
SDSSJ002927.38+254401.7	BELLS	0.5869	2.4504	1.34	241 \pm 45	Shu et al. (2016)
SDSSJ020121.39+322829.6	BELLS	0.3957	2.8209	1.70	256 \pm 20	Shu et al. (2016)
SDSSJ023740.63–064112.9	BELLS	0.4859	2.2491	0.65	290 \pm 89	Shu et al. (2016)
SDSSJ074249.68+334148.9	BELLS	0.4936	2.3633	1.22	218 \pm 28	Shu et al. (2016)
SDSSJ075523.52+344539.5	BELLS	0.7224	2.6347	2.05	272 \pm 52	Shu et al. (2016)
SDSSJ085621.59+201040.5	BELLS	0.5074	2.2335	0.98	334 \pm 54	Shu et al. (2016)
SDSSJ091807.86+451856.7	BELLS	0.5238	2.3440	0.77	119 \pm 61	Shu et al. (2016)
SDSSJ091859.21+510452.5	BELLS	0.5811	2.4030	1.60	298 \pm 49	Shu et al. (2016)
SDSSJ111027.11+280838.4	BELLS	0.6073	2.3999	0.98	191 \pm 39	Shu et al. (2016)
SDSSJ111634.55+091503.0	BELLS	0.5501	2.4536	1.03	274 \pm 55	Shu et al. (2016)
SDSSJ114154.71+221628.8	BELLS	0.5858	2.7624	1.27	285 \pm 44	Shu et al. (2016)
SDSSJ120159.02+474323.2	BELLS	0.5628	2.1258	1.18	239 \pm 43	Shu et al. (2016)
SDSSJ122656.45+545739.0	BELLS	0.4980	2.7322	1.37	248 \pm 26	Shu et al. (2016)
SDSSJ222825.76+120503.9	BELLS	0.5305	2.8324	1.28	255 \pm 50	Shu et al. (2016)
SDSSJ234248.68–012032.5	BELLS	0.5270	2.2649	1.11	274 \pm 43	Shu et al. (2016)
SL2SJ020457–110309	SL2S	0.609	1.89	0.54 \pm 0.07	250 \pm 30	Sonnenfeld et al. (2015)
SL2SJ020524–093023	SL2S	0.557	1.33	0.76 \pm 0.09	276 \pm 37	Sonnenfeld et al. (2015)
SL2SJ021801–080247	SL2S	0.884	2.06	1.00 \pm 0.03	246 \pm 48	Sonnenfeld et al. (2015, 2013a)
SL2SJ023307–043838	SL2S	0.671	1.87	1.77 \pm 0.06	204 \pm 21	Sonnenfeld et al. (2015)
SDSSJ0143–1006	SLACS	0.2210	1.1046	1.23	203 \pm 17	Shu et al. (2017)
SDSSJ0159–0006	SLACS	0.1584	0.7477	0.92	216 \pm 18	Shu et al. (2017)
SDSSJ0324+0045	SLACS	0.3210	0.9199	0.55	183 \pm 19	Shu et al. (2017)
SDSSJ0324–0110	SLACS	0.4456	0.6239	0.63	310 \pm 38	Shu et al. (2017)
SDSSJ0753+3416	SLACS	0.1371	0.9628	1.23	208 \pm 12	Shu et al. (2017)
SDSSJ0754+1927	SLACS	0.1534	0.7401	1.04	193 \pm 16	Shu et al. (2017)
SDSSJ0757+1956	SLACS	0.1206	0.8326	1.62	206 \pm 11	Shu et al. (2017)
SDSSJ0826+5630	SLACS	0.1318	1.2907	1.01	163 \pm 8	Shu et al. (2017)
SDSSJ0847+2348	SLACS	0.1551	0.5327	0.96	199 \pm 16	Shu et al. (2017)
SDSSJ0851+0505	SLACS	0.1276	0.6371	0.91	175 \pm 11	Shu et al. (2017)
SDSSJ0920+3028	SLACS	0.2881	0.3918	0.70	297 \pm 17	Shu et al. (2017)
SDSSJ0955+3014	SLACS	0.3214	0.4671	0.54	271 \pm 33	Shu et al. (2017)
SDSSJ0956+5539	SLACS	0.1959	0.8483	1.17	188 \pm 11	Shu et al. (2017)
SDSSJ1010+3124	SLACS	0.1668	0.4245	1.14	221 \pm 11	Shu et al. (2017)
SDSSJ1031+3026	SLACS	0.1671	0.7469	0.88	197 \pm 13	Shu et al. (2017)
SDSSJ1040+3626	SLACS	0.1225	0.2846	0.59	186 \pm 10	Shu et al. (2017)
SDSSJ1041+0112	SLACS	0.1006	0.2172	0.60	200 \pm 7	Shu et al. (2017)
SDSSJ1048+1313	SLACS	0.1330	0.6679	1.18	195 \pm 10	Shu et al. (2017)
SDSSJ1051+4439	SLACS	0.1634	0.5380	0.99	216 \pm 16	Shu et al. (2017)
SDSSJ1056+4141	SLACS	0.1343	0.8318	0.72	157 \pm 10	Shu et al. (2017)
SDSSJ1101+1523	SLACS	0.1780	0.5169	1.18	270 \pm 15	Shu et al. (2017)
SDSSJ1116+0729	SLACS	0.1697	0.6860	0.82	190 \pm 11	Shu et al. (2017)
SDSSJ1127+2312	SLACS	0.1303	0.3610	1.25	230 \pm 9	Shu et al. (2017)
SDSSJ1137+1818	SLACS	0.1241	0.4627	1.29	222 \pm 8	Shu et al. (2017)
SDSSJ1142+2509	SLACS	0.1640	0.6595	0.79	159 \pm 10	Shu et al. (2017)
SDSSJ1144+0436	SLACS	0.1036	0.2551	0.76	207 \pm 14	Shu et al. (2017)
SDSSJ1213+2930	SLACS	0.0906	0.5954	1.35	232 \pm 7	Shu et al. (2017)
SDSSJ1301+0834	SLACS	0.0902	0.5331	1.00	178 \pm 8	Shu et al. (2017)
SDSSJ1330+1750	SLACS	0.2074	0.3717	1.01	250 \pm 12	Shu et al. (2017)
SDSSJ1403+3309	SLACS	0.0625	0.7720	1.02	190 \pm 6	Shu et al. (2017)
SDSSJ1430+6104	SLACS	0.1688	0.6537	1.00	180 \pm 15	Shu et al. (2017)
SDSSJ1433+2835	SLACS	0.0912	0.4115	1.53	230 \pm 6	Shu et al. (2017)
SDSSJ1541+3642	SLACS	0.1406	0.7389	1.17	194 \pm 11	Shu et al. (2017)
SDSSJ1543+2202	SLACS	0.2681	0.3966	0.78	285 \pm 16	Shu et al. (2017)
SDSSJ1550+2020	SLACS	0.1351	0.3501	1.01	243 \pm 9	Shu et al. (2017)
SDSSJ1553+3004	SLACS	0.1604	0.5663	0.84	194 \pm 15	Shu et al. (2017)
SDSSJ1607+2147	SLACS	0.2089	0.4865	0.57	197 \pm 16	Shu et al. (2017)
SDSSJ1633+1441	SLACS	0.1281	0.5804	1.39	231 \pm 9	Shu et al. (2017)
SDSSJ2309–0039	SLACS	0.2905	1.0048	1.14	184 \pm 13	Shu et al. (2017)

Table A1 – *continued*

system name	survey	zl	zs	$\theta_E(\prime)$	σ_0 (Km s $^{-1}$)	reference
SDSSJ2324+0105	SLACS	0.1899	0.2775	0.59	245 \pm 15	Shu et al. (2017)
Q0142-100	CASTLES	0.491	2.719	1.12	246 $^{+17}_{-47}$	Rusin et al. (2003a) Leier et al. (2011)
MG0414+0534	CASTLES	0.958	2.639	1.19	247 $^{+10}_{-13}$	Rusin et al. (2003a) Leier et al. (2011)
B0712+472	CASTLES	0.406	1.339	0.71	164 \pm 7	Rusin et al. (2003a) Leier et al. (2011)
HS0818+1227	CASTLES	0.390	3.115	1.42	246 $^{+17}_{-42}$	Rusin et al. (2003a) Leier et al. (2011)
B1030+074	CASTLES	0.599	1.535	0.78	257 $^{+10}_{-18}$	Rusin et al. (2003a) Leier et al. (2011)
HE1104-1805	CASTLES	0.729	2.303	1.595	303 $^{+11}_{-10}$	Rusin et al. (2003a) Leier et al. (2011)
B1608+656	CASTLES	0.630	1.394	1.135	267 $^{+6}_{-15}$	Rusin et al. (2003a) Leier et al. (2011)
HE2149-2745	CASTLES	0.603	2.033	0.85	191 $^{+9}_{-9}$	Rusin et al. (2003a) Leier et al. (2011)
MG1549+3047	CASTLES	0.111	1.170	1.15	227 \pm 18	Rusin et al. (2003a) Lehar et al. (1996)

System Name	D^{obs}	$\theta_E(\prime)$	Flag
SDSSJ1318-0313	1.207548476671243	1.58	
SDSSJ0801+4727	1.7690928325399644	0.49	†
SDSSJ1234-0241	1.234704134938535	0.53	†
SDSSJ1352+3216	2.4345927827771154	1.82	†
SDSSJ0008-0004	1.079816763956848	1.16	†
SDSSJ0252+0039	1.3407639908720494	1.04	†
SDSSJ0405-0455	1.0835693599307283	0.8	†
SDSSJ1100+5329	1.5071867558989571	1.52	
SDSSJ1218+0830	1.0483021267443504	1.45	
SDSSJ2238-0754	1.123259330363861	1.27	†
SDSSJ2341+0000	1.1652751780813544	1.44	†
SL2SJ022511-045433	1.1145194380761674	1.76	
SL2SJ090407-005952	1.4495478313743804	1.40	
SL2SJ220329+020518	1.4903288161448882	1.95	†
SL2SJ221326-000946	1.362770060019399	1.07	†
SL2SJ222012+010606	4.643580764983071	2.16	†
SL2SJ222217+001202	1.022314778682008	1.44	†
SDSSJ091807.86+451856.7	1.8853999737796163	0.77	†
SL2SJ023307-043838	1.4747541461571618	1.77	
SDSSJ0143-1006	1.0349508604157698	1.23	
SDSSJ0757+1956	1.323692987529667	1.62	†
SDSSJ0826+5630	1.318113655499309	1.01	†
SDSSJ0851+0505	1.0303196656712754	0.91	†
SDSSJ0956+5539	1.147828113281079	1.17	†
SDSSJ1048+1313	1.0760178574880814	1.18	
SDSSJ1056+4141	1.0128377643232576	0.72	†
SDSSJ1142+2509	1.0835264989141573	0.79	†
SDSSJ1301+0834	1.094376326151474	1.0	†
SDSSJ1430+6104	1.0701919604254106	1.0	†
SDSSJ1433+2835	1.0028649501362656	1.53	†
SDSSJ1541+3642	1.0779263693220975	1.17	†
SDSSJ2309-0039	1.1675511061635446	1.14	

Table A2. 32 gravitational lens systems with $D^{obs} > 1$.

et al. (1984). Since not all the obtained z_l were physically possible, the final sample was reduced to 788 lenses. Later, we randomly associate to each one of the 788 lenses, their parameters, i. e., velocity dispersion ($98 < \sigma < 342$), ellipticity ($0.5 < \epsilon < 0.9$), position angle ($0^\circ < \theta < 180^\circ$), and external shear ($0. < \gamma < 0.2$). In addition, following the same procedure, we have simulated SLS assuming an isothermal and elliptical power-law mass distribution, with a slope α between $1.6 < \alpha < 2.6$ obtaining ~ 788 systems. We considered the definition for the Einstein radius following the work of Vegetti et al. (2014) for both approaches. Finally, these mock SLS were fitted using the GRAVLENS code (Keeton 2011) using a SIE model, and assuming a Λ CDM Cosmology ($\Lambda = 0.73$, $\Omega_m = 0.27$, $h = 0.7$). Figure C1 shows the histograms of the relative error between the simulated Einstein

radius (from the SIE and SIE+ α lens models, and assuming a SIS SIS+ α) and the fitted SIE Einstein radius. In addition, we overplot the cumulative distribution function (CDF) for all the cases. The comparison (through the relative error) between the simulated SIE θ_E , and the fitted one, gives as a result that approximately the 80% of the sample have an error less than the 10%. However, comparing the simulated SIE+ α θ_E and the fitted SIE θ_E , gives an error of $\sim 35\%$ or less for the majority of the data (80%). On the other hand, when we compare the simulated θ_E (assuming a SIS) with the θ_E obtained from the fit, we obtain that approximately the 80% of the objects have an error less than the 25%. Moreover, when the SIS+ α θ_E is compared with the fitted SIE, the error increases to 45% or less for the 80% of the objects. We can interpret these results as follows. If we

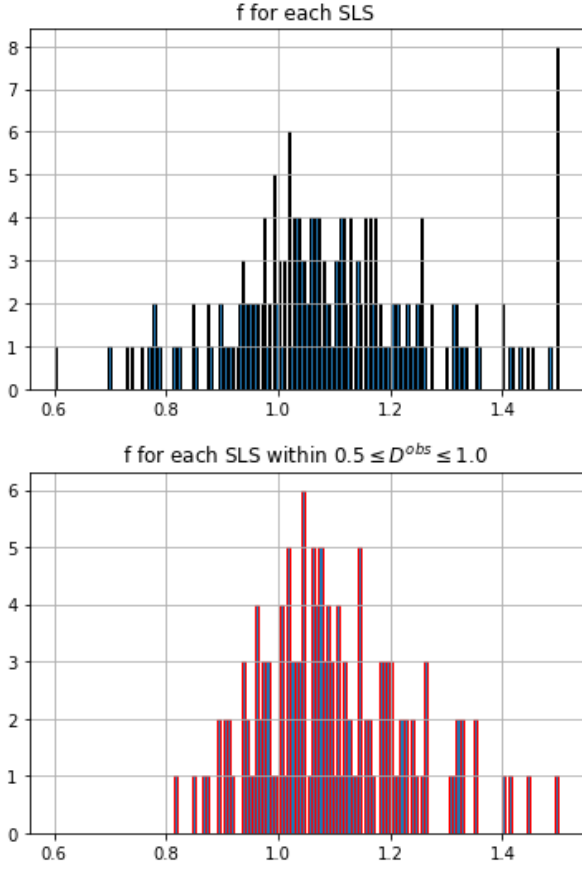


Figure B1. Probability density function (PDF) histogram of the best fit values of f for the complete sample (top panel) and the SS3 sample $0.5 < D^{obs} < 1$ (bottom panel) for the ω CDM model, assuming f as an individual and free parameter for each SLS.

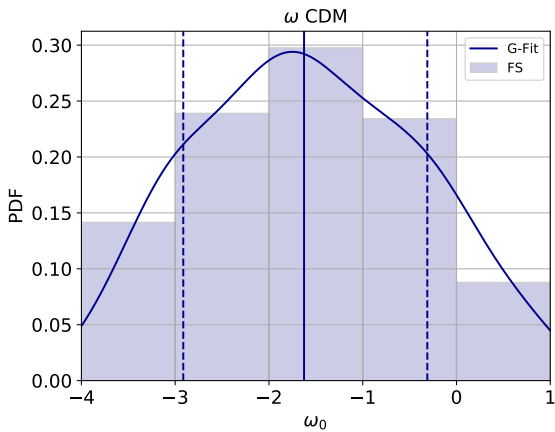


Figure B2. Histogram of the best fit values of ω_0 for the FS sample (ω CDM model). The continuous line represents a Gaussian kernel fit. The mean value is indicated with a vertical solid line, and with dashed vertical lines the 1σ values.

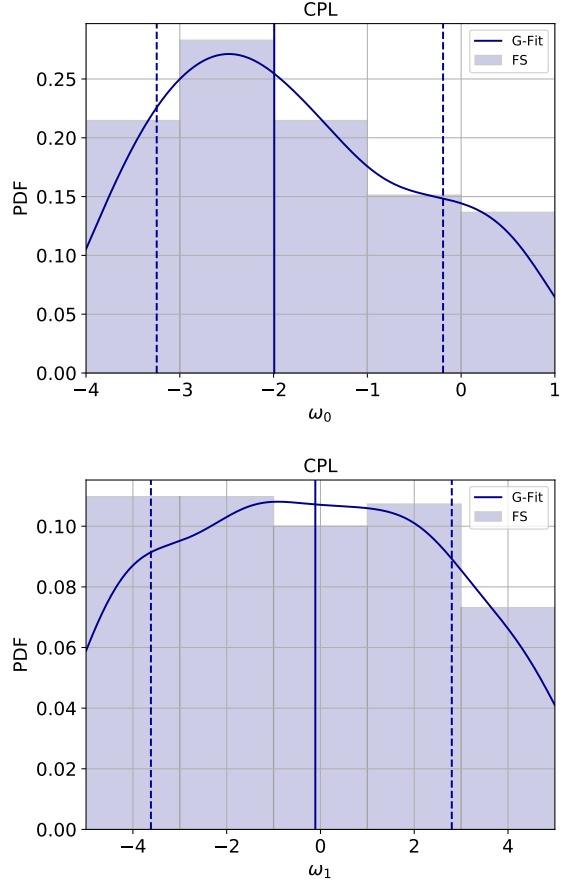


Figure B3. Histogram of the best fit values of ω_0 (top panel) and ω_1 (bottom panel) of the FS in the CPL model. The continuous line represents a Gaussian kernel fit. The mean value is indicated with a vertical solid line, and with dashed vertical lines the 1σ values.

adopt a simple SIS θ_E to characterize a lens, we could have a worse estimate of the lens mass, i.e. we will have a bigger scatter on the value of the velocity dispersion of the lens. This scatter could be inherited to the corrective parameter f used in Eq. (7). Moreover, assuming a power-law mass distribution with a SIS or SIE lens model, the lens mass can not be modeled accurately enough obtaining a worst estimate on the value of the velocity dispersion. These results can be related to the values obtained for the f parameter considered as an independent free parameter for each system (see appendix B), in which some systems are outside the range proposed by Ofek et al. (2003). This problem could be addressed by both including an external shear parameter in complex systems (i.e. quadruply lensed quasars, systems with lensed arcs) and by estimating cosmological parameters and lens modelling simultaneously. Even though some simulated systems present a bigger scatter with respect to the fitted SIE θ_E , neither of these systems shows a nonphysical value for the observational lens equation.

This paper has been typeset from a $\text{\TeX}/\text{\LaTeX}$ file prepared by the author.

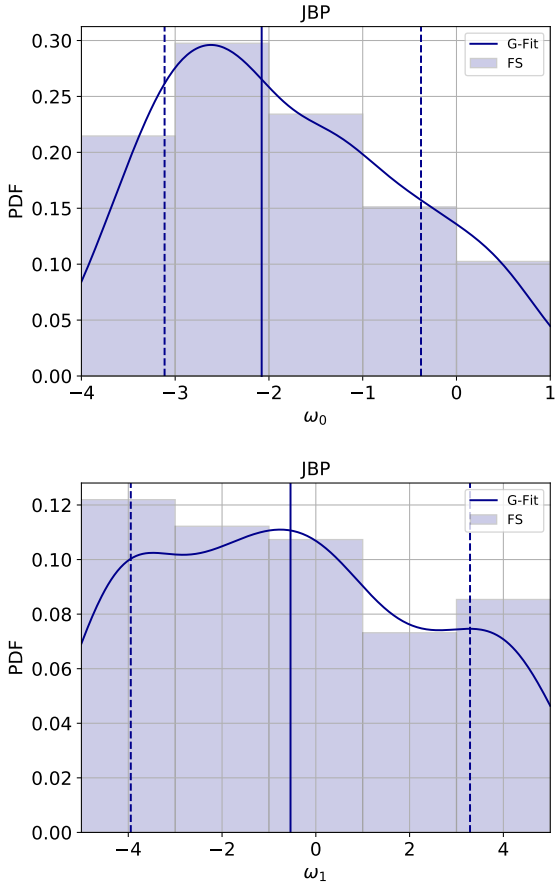


Figure B4. Histogram of the best fit values of ω_0 (top panel) and ω_1 (bottom panel) of the FS for the JBP model. The continuous line represents a Gaussian kernel fit. The mean value is indicated with a vertical solid line, and with dashed vertical lines the 1σ values.

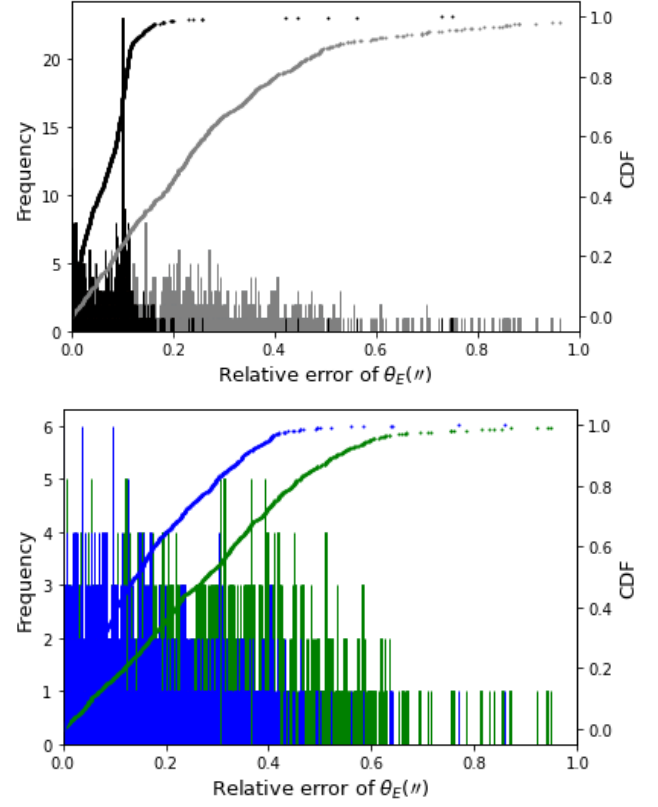


Figure C1. Relative error's histograms. *Top panel.*- Calculated using the simulated θ_E assuming a SIE and SIE+ α , (black and gray colors respectively), and the θ_E from a SIE model fitting. *Bottom panel.*- Calculated using the simulated θ_E (assuming a SIS and SIS+ α , blue and green colors respectively) and the θ_E from a SIE model fitting. The dotted line in both panels shows the cumulative distribution function (CDF).